Spontaneous rupture of surfactant-covered thin liquid sheets

Hansol Wee, Brayden W. Wagoner, and Osman A. Basaran*
Davidson School of Chemical Engineering, Purdue University, West Lafayette, Indiana 47907, USA

(Received 2 July 2022; accepted 7 September 2022; published 29 September 2022)

Rupture of thin free films of Newtonian fluids is analyzed when the sheets' two free surfaces are covered with insoluble surfactant and surface rheological effects are important. The analysis relies on a long-wavelength model composed of a system of one-dimensional evolution equations for film thickness $h(z,t)$, lateral velocity $v(z,t)$, and surfactant concentration $\Gamma(z,t)$ (z: lateral coordinate, t: time). As the dynamics near the space-time singularity in sheet rupture is asymptotically self-similar when surfactants are convected away from the rupture point, the partial differential equations are also reduced to a set of ordinary differential equations in similarity space. For both highly viscous fluids in the Stokes limit and moderately viscous fluids, it is shown that the dominant balance involves van der Waals pressure and bulk viscous as well as surface viscous stresses while surface tension pressure and Marangoni stress are negligible. In the Stokes limit, self-similarity is of the second kind and $h \sim \Gamma \sim \tau^{1/3}$, $z \sim \tau^{\alpha_z}$, and $v \sim \tau^{\alpha_z - 1}$ where τ is time remaining until rupture and α_z is the lateral scaling exponent. Although α_z cannot be determined by dimensional arguments, it is shown to equal 0.249. For moderately viscous fluids, inertia also enters the picture and self-similarity is of the first kind ($h \sim \Gamma \sim \tau^{1/3}$, $z \sim \tau^{1/2}$, and $v \sim \tau^{-1/2}$). Scalings determined from theory are confirmed by numerical solution of the evolution equations. Closed-form expressions for the sheet's thinning rate, which have heretofore been lacking, are also reported.

DOI: 10.1103/PhysRevFluids.7.094005

I. INTRODUCTION

Thinning and rupture of liquid films play a central role in diverse technological applications and nature [1–3]. In a free liquid film or a liquid sheet, which has two free surfaces and is surrounded by air or another liquid, if the thickness of the film is less than the order of a micrometer, long-range intermolecular van der Waals attractive forces between the molecules in the liquid film can become significant and influence the thinning dynamics [4,5]. Indeed, van der Waals attractive forces can cause the film to destabilize and rupture despite the stabilizing action of surface tension if the film is tens to hundreds of nanometers in thickness. For films of thickness of the order of μm or larger, van der Waals forces are not operative, and hence, not responsible for film rupture [6]. A striking example of sheet rupture is provided in the paper by Debrégeas *et al.* [7] who observed it while studying experimentally the bursting of bubbles at air–liquid interfaces. These authors have reported that the liquid sheet that forms between the bubble and the interface spontaneously ruptures below a thickness of 70 nm due to van der Waals forces. The destabilizing van der Waals attractive forces in liquid sheets are key to controlling foam instability due to sheet rupture [8], emulsion stability due to drop coalescence [9,10], and bubble coalescence in gas-liquid dispersions [11] (also, see below). They also play a key role in determining appropriate operating conditions for preventing film rupture in industrial processes such as manufacturing of polymer films [12] and curtain coating [13].

*obasaran@purdue.edu

Similarly, van der Waals attraction between the molecules in the liquid and a solid can cause rupture of films deposited on solid surfaces, which have one free surface, and is crucial to understanding of the formation of dry spots in diverse coating flows [14,15] and the rupture of the tear film covering the cornea [16].

In many of the aforementioned applications involving sheet rupture as well as in a plethora of other free-surface or interfacial flows, surfactants are often present by design, e.g., as in spraying applications [17] but also sometimes as undesirable contaminants. A primary action of surfactants in these flows is attributable to their preferential adsorption onto interfaces and the concomitant lowering of surface tension, and hence capillary pressure [18,19]. However, surfactant concentration is often nonuniform at an interface in a free-surface flow. The nonuniformity is caused by changes in interfacial area by compression or expansion due to normal dilatation as well as tangential stretching, and also because of surfactant transport by convection and diffusion. Gradients in surfactant concentration give rise to gradients in surface tension and hence tangential interfacial or Marangoni stresses [20–22]. The Marangoni effect is perhaps the most studied consequence of surfactants, and manifests itself and brings about rich physics in problems as diverse as interfacial turbulence in mass transfer, tears of wine, microthread cascades in drop and jet breakup, inkjet printing, droplet bouncing, and evaporating colloidal droplets [20,23–27]. However, lowering of surface tension, which is often referred to as the solutocapillary effect, and gradients in surface tension, or the Marangoni effect, may not be the sole consequences of surfactants at interfaces. Surfactants may also induce surface rheological or viscous effects [19] as surfactant molecules are transported along an interface and give rise to frictional losses as the molecules deform against one another [28]. While the implication of these effects has been investigated in a number of film flows such as coating flows [18,29–31], only a handful of studies to date have considered the effects of surface rheology on sheet rupture (see below). The major goal of this paper is to advance the understanding of the effects of surface viscosities on the finite-time hydrodynamic singularity that arises as a liquid sheet of initial thickness of the order of a micrometer or less and whose two surfaces are initially uniformly covered with surfactant begins to thin spontaneously and tends toward rupture.

Consider a quiescent liquid sheet of a pure fluid of uniform thickness $2\tilde{h}_i$ that is surrounded by a passive gas, e.g., air. The surface tension of the liquid-gas interface is denoted by σ_p. We note that if the undisturbed thickness of the sheet is one micrometer, the gravitational Bond number $\mathrm{Bo} \equiv \rho g(2\tilde{h}_i)^2/\sigma_p$, where ρ is the density of the film liquid and g is the acceleration due to gravity, that measures the relative importance of gravitational to surface tension force is 1.4×10^{-7} for a water film. Therefore, for such a sufficiently thin sheet, the pressure within the film is uniform and exceeds the exterior pressure by $A_H/[6\pi(2\tilde{h}_i)^3]$, where A_H is the Hamaker constant, due to van der Waals attraction between the molecules in the film. Next consider that the two surfaces of the sheet are subjected to two-dimensional, sinusoidal perturbations of amplitude ε and wavelength $\tilde{\lambda}$ that are symmetric about the mid-plane of the film. When subjected to such perturbations, surface tension causes the pressure to rise (fall) underneath the peaks (valleys) of the disturbed free surface since the surface tension-induced capillary pressure equals the surface tension σ_p times the curvature. The difference in the capillary pressure between the peaks and the valleys scales as $\sigma_p(\varepsilon\tilde{h}_i/\tilde{\lambda}^2)$. By contrast, van der Waals attraction between the molecules of the film causes the pressure to rise underneath the valleys and to fall underneath the peaks of the perturbed free surface. The difference in the van der Waals-induced pressure between the valleys and the peaks scales as $\varepsilon(A_H/\tilde{h}_i^3)$. Balancing the stabilizing capillary pressure and the destabilizing van der Waals pressure yields that there is a critical wavelength $\tilde{\lambda}_c \sim \tilde{h}_i^2/d$, where $d \equiv \sqrt{A_H/\sigma_p}$ is of the order of the molecular length scale: the sheet is unstable with respect to disturbances of wavelengths exceeding $\tilde{\lambda}_c$ whereas it is stable when $\tilde{\lambda} < \tilde{\lambda}_c$. As $\tilde{h}_i$ is of the order of micrometers and d is of the order of nanometers, $\tilde{\lambda}_c/\tilde{h}_i \sim \tilde{h}_i/d \gg 1$ and therefore the instability is a long-wavelength one. Sheludko [32] and later Vrij [33] (see also the review by Sheludko [34]), who both used energy arguments, and subsequently Ruckenstein and Jain [35], who carried out a hydrodynamic linear stability analysis, have shown that the exact value of the critical wavelength is $\tilde{\lambda}_c = 8\pi^{3/2}\tilde{h}_i^2/d$.

Erneux and Davis [36] made use of the long-wavelength nature of the problem, and derived and solved a set of one-dimensional (1D) evolution equations to analyze Newtonian film rupture. These authors showed that nonlinear effects led to acceleration of thinning and resulted in rupture times that are much smaller than those predicted by linear theory. In film rupture, the dynamics close to the space-time singularity $(\tilde{z}_R, \tilde{t}_R)$, where $\tilde{z}_R$ and $\tilde{t}_R$ are the lateral location $\tilde{z}$ and time $\tilde{t}$ at which the film ruptures, is set solely by the approach to the singularity. As the finite-time singularity is approached, the film half-thickness $\tilde{h}$, the lateral length scale $\tilde{z}' = \tilde{z} - \tilde{z}_R$, and the timescale $\tilde{\tau} = \tilde{t}_R - \tilde{t}$, which is the time remaining until rupture, will be orders of magnitude smaller in the vicinity of the rupture point than those in the far field. Therefore, the rupture dynamics is expected to be self-similar and described in terms of similarity solutions. Following an early numerical study by Ida and Miksis [37], Vaynblat *et al.* [38] carried out a combined theoretical and numerical analysis that focused on the self-similar dynamics that arises during rupture of sheets of Newtonian fluids. These authors analyzed by using a set of 1D evolution equations the thinning and pinch-off of Newtonian sheets undergoing line—sometimes also referred to as two-dimensional—as well as point—also referred to as axisymmetric—rupture. Vaynblat *et al.* [38] showed using kinematic and dynamic balance arguments that the asymptotic balance of forces is between inertial, viscous, and van der Waals forces while surface tension force is negligible. These authors further showed that the self-similarity is of the first kind [39] and that the film half-thickness, lateral length scale $\tilde{z}'$, and lateral velocity $\tilde{v}$ vary with time until rupture as $\tilde{h} \sim \tilde{\tau}^{1/3}$, $\tilde{z}' \sim \tilde{\tau}^{1/2}$, and $\tilde{v} \sim \tilde{\tau}^{-1/2}$.

More recently, Thete *et al.* [40] have analyzed the self-similar dynamics of rupture of Newtonian sheets undergoing Stokes and inviscid flow. For sheets with negligible inertia, Thete *et al.* [40] have shown that the dominant balance of forces involves solely viscous and van der Waals forces, with capillary force remaining negligible throughout the thinning process, and the self-similarity is of the second kind [39]. These authors have shown that in this viscous or Stokes flow regime, the film half-thickness, lateral length scale, and lateral velocity vary with time until rupture as $\tilde{h} \sim \tilde{\tau}^{1/3}$, $\tilde{z}' \sim \tilde{\tau}^{0.26}$, and $\tilde{v} \sim \tilde{\tau}^{-0.74}$. However, for a sheet of an inviscid fluid for which the effect of viscosity is negligible, it was shown that the dominant balance of forces is between inertial, capillary, and van der Waals forces as the film evolves towards rupture, and the self-similarity is of the first kind [39]. In this inviscid regime, the film half-thickness, lateral length scale, and lateral velocity vary with time until rupture as $\tilde{h} \sim \tilde{\tau}^{2/7}$, $\tilde{z}' \sim \tilde{\tau}^{4/7}$, and $\tilde{v} \sim \tilde{\tau}^{-3/7}$. Furthermore, it was also shown by these authors that as real fluids have finite viscosity, the aforementioned viscous and inertial regimes are only transitory and can only describe the initial thinning dynamics of highly viscous and slightly viscous sheets, respectively. Moreover, Thete *et al.* [40] have further demonstrated that regardless of the fluid's viscosity, for sheets that initially thin in either of these two regimes, their dynamics eventually transition to a late stage or final inertial-viscous regime in which inertial, viscous, and van der Waals forces balance each other while capillary force remains negligible, in accordance with the results of Vaynblat *et al.* [38].

Effects of surfactants on rupture of Newtonian sheets have been studied by Matar [41] and more recently by Choudhury *et al.* [42]. Matar [41] considered situations when surface viscosity is absent ($\eta = 0$ where η stands for the dimensionless surface viscosity) and also ones in which surface viscosity is independent of surfactant concentration or is a constant ($\eta = 1$). Choudhury *et al.* [42] considered situations when surface viscosity is absent but also ones in which surface viscosity is either a constant or a function of surfactant concentration. In their notation, $\eta = 1 + \beta(\Gamma - 1)$, where the dimensionless parameter $0 \leqslant \beta \leqslant 1$ and Γ is the dimensionless concentration of surfactant at the interface. Thus, $\beta = 0$ reduces to the case of constant surface viscosity. When $\beta = 1$, $\eta = \Gamma$, i.e., surface viscosity equals surfactant concentration but vanishes where there is no surfactant—a constitutive relation that has been widely adopted in the recent literature (see below). However, for $0 < \beta < 1$, surface viscosity is not only a function of surfactant concentration but nonzero even where $\Gamma = 0$. Choudhury *et al.* [42] have explicitly stated that regardless of the thinning dynamics that the sheet may exhibit as it tends toward rupture, capillary and Marangoni forces are always negligible near pinch-off. Matar [41] and Choudhury *et al.* [42] both found that in the absence of surface viscosity, the dominant balance of forces is between van der Waals,

inertial, and bulk viscous forces and $\tilde{h} \sim \tilde{\tau}^{1/3}$, $\tilde{z}' \sim \tilde{\tau}^{1/2}$, $\tilde{v} \sim \tilde{\tau}^{-1/2}$, and $\tilde{\Gamma} \sim \tilde{\tau}^{1/3}$ ($\tilde{\Gamma}$: dimensional surfactant concentration). In situations in which surface viscosity is present, Matar [41]—when surface viscosity is constant—and Choudhury *et al.* [42]—when surface viscosity is either a constant ($\beta = 0$) or a function of Γ but $\beta \neq 1$—both found that the dominant balance of forces is between van der Waals, inertial and surface viscous forces while bulk viscous force is negligible. Under the aforementioned balance of forces, $\tilde{h} \sim \tilde{\tau}^{1/2}$, $\tilde{z} \sim \tilde{\tau}^{1/4}$, $\tilde{v} \sim \tilde{\tau}^{-3/4}$, and $\tilde{\Gamma} \sim \tilde{\tau}^{1/2}$. From the standpoint of the present paper, the most interesting and relevant case considered by Choudhury *et al.* [42] is that when $\beta = 1$ so that $\eta \sim \Gamma$. In this case, Choudhury *et al.* [42] found that the dominant balance is between van der Waals, inertial and bulk viscous forces—the same as in the absence of surfactants or when surfactants are present but surface viscous effects are absent—and surface viscous force is asymptotically negligible as the sheet tends toward rupture (but see below).

In this paper, we consider situations in which the two free surfaces of a thin sheet of a Newtonian fluid are initially covered uniformly with a monolayer of insoluble surfactant and surface rheological effects are important. It should be emphasized that we are concerned in this work with the spontaneous rupture of a surfactant-covered liquid sheet after its two free surfaces have been subjected to perturbations of infinitesimal amplitude. In this context, the presence of van der Waals forces is crucial for film rupture as has already been explained above (but also see below). However, when the interfaces of the sheet are subjected to perturbations of sufficiently large amplitude, it has been shown that the film can rupture without van der Waals forces. Perhaps the best-known example of such a situation can be found in the work of Burton and Taborek [43]. In that paper, the authors showed that an inviscid free film can undergo finite-time pinch-off (rupture) due to nonlinear Bernoulli effects. However, for films of finite viscosity in the absence of van der Waals forces, the films do not exhibit rupture because of the dissipative effect of viscosity [36,44]. Indeed, it has been specifically stated by Bowen and Tilley [45] that when viscous stresses are included in the system of 1d inviscid sheet equations, the resulting evolution equations are dissipative in nature and additional physical effects need to be introduced in order for the sheet to rupture.

However, if the films are initially subjected to large surface tension gradients due to either chemical or thermal inhomogeneity, it has been shown that the concomitant strong Marangoni stress-driven flows can induce rupture in the absence of van der Waals forces [6,45,46]. Furthermore, it has also been shown that film rupture can only occur for sufficiently large values of the Marangoni number [45,46]. In this paper, however, we focus on sheet rupture not only when the Marangoni number is small but also when surfactants initially cover the interface uniformly, i.e., in the absence of an initial Marangoni stress.

Following recent works on the closely related problem of the breakup of surfactant-covered jets [47–49], we adopt the physically-based ansatz that surface viscosity is a function of surfactant concentration but that it vanishes where surfactant concentration also vanishes. To fix ideas, we focus our attention in this paper on the dynamics of sheet rupture in two situations: when the film fluid is (1) highly viscous so that the sheet is undergoing Stokes flow and (2) moderately viscous so that inertia cannot be neglected. In free-surface flows involving transport of an insoluble surfactant at an interface, the relative importance of surfactant transport by convection to that by diffusion is given by the Peclet number Pe. As discussed in the experimental and computational study by Liao *et al.* [50], the value of Pe for common surfactants would range between several hundred and several million because of the low values of surfactant diffusivities which lie between 10^{-6} and 10^{-5} cm^2/s. Therefore, we take Pe $\gg 1$ in the remainder of this article. The analysis employed herein relies on the use of a long-wavelength model composed of a system of spatially one-dimensional evolution equations for film half-thickness $\tilde{h}$, lateral velocity $\tilde{v}$ and surfactant concentration $\tilde{\Gamma}$. As the dynamics near the space-time singularity where the film ruptures is asymptotically self-similar when surfactants are convected away from the rupture point, the transient partial differential evolution equations are also reduced to a set of ordinary differential equations in similarity space. In the Stokes limit, it is shown that self-similarity is of the second kind [39] and the dominant balance of forces involves van der Waals pressure that drives rupture and bulk viscous as well as surface viscous

stresses while surface tension pressure and Marangoni stress are negligible. For moderately viscous fluids, inertia also enters the picture and self-similarity is of the first kind [39]. Therefore, in contrast to earlier work [42], we demonstrate that surface viscous stresses are asymptotically important at breakup even as surfactant is depleted from the rupture location. Moreover, closed-form expressions are also obtained for the minimum sheet thickness and/or the sheet's thinning rate in both situations, a result that had been lacking in earlier studies. Given their simple forms, these analytical results can be readily used to infer surface viscosity from experiments.

In this work, as in Refs. [41] and [42], we treat the surfactant as being insoluble and hence confined to the liquid-gas interface. However, it has been shown in Ref. [24] and elsewhere that the solubility of common surfactants like sodium dodecyl sulfate (SDS) in glycerol-water mixtures, which are widely used in experiments on pinch-off [24,50], does not affect the surface tension or its gradient along the interface in studying breakup as the surface-adsorption dynamics of the surfactant is at least two orders of magnitude slower than the flow dynamics or the timescale over which rupture takes place. Moreover, in Ref. [50], the authors have shown how the insoluble surfactant limit can be realized in laboratory experiments involving pinch-off.

In this paper, as in earlier studies of rupture singularities that arise during the breakup of surfactant-covered liquid sheets [41,42], it is taken that only van der Waals interactions are important in determining the disjoining pressure within the film. However, it is well known that intermolecular forces other than van der Waals forces may also play a role in thin film flows in situations as diverse as the rupture of supported and free films, drop and bubble coalescence, and spreading (see, e.g., Refs. [11,19,51,52]). In particular, another possible contributor to disjoining pressure is electrostatic force that may exist in aqueous thin films containing ionic surfactants [19]. However, the mechanism(s) for film rupture (is) are not yet clear in all situations. As articulated by Langevin [11], the mechanisms for bubble coalescence, where a thin film separates two bubbles prior to their merging, are now well understood in the absence of surfactants even for salt solutions. However, Langevin [11] has also noted that a complete model is not yet available for surfactant solutions. Therefore, in this paper we assume that the surfactants are nonionic and that the sole contribution to the intermolecular or thin-film forces comes from van der Waals forces. We further note that this assumption has also been adopted by Dai and Leal [53] and Vannozzi [54] who have carried out detailed boundary integral simulations of the coalescence of surfactant-laden drops.

The paper is organized as follows. Section II describes the mathematical formulation of the problem. First, the two-dimensional (2D) system of equations, boundary conditions, and initial conditions governing the thinning and rupture of a Newtonian sheet whose surface is covered with a monolayer of insoluble surfactant is presented. Next, since the instability leading to sheet rupture is a long-wavelength one and the profile of the sheet in the vicinity of the rupture singularity is expected to be slender, a spatially one-dimensional (1D) set of slender-sheet evolution equations are derived that governs the dynamics of thinning and breakup. In the following section (Sec. III), sheet thinning and rupture are analyzed in the limit of Stokes flow when $\mathrm{Pe} = \infty$. First, the 1D evolution equations in physical space are cast into similarity space by adopting the similarity ansatz and that all variables have simple power-law dependencies on time remaining until rupture. As the analysis of rupture for sheets undergoing Stokes flow leads to a self-similarity of the second kind, one of the scaling exponents is left undetermined and the analysis in this case leads to a more complicated mathematical problem than that in which inertia is important (see below). In lieu of using numerical solutions of the evolution equations as was done in the original analysis of jet breakup [55] and sheet rupture [40] in Stokes flow, we determine analytically the value of the missing scaling exponent. In the following section, we present numerical solutions of the evolution equations and also confirm the theoretical predictions made in the earlier sections of the paper. In the next section (Sec. IV), sheet thinning and rupture are analyzed in situations in which inertia cannot be neglected when $\mathrm{Pe} = \infty$. Here, the analysis leads to a self-similarity of the first kind and all scaling exponents can be readily determined by dimensionality arguments. In the next section (Sec. V), we relax the assumption of infinite Peclet number and consider the dynamics of sheet rupture at large but finite Pe. In the following section (Sec. VI), we provide a physically based

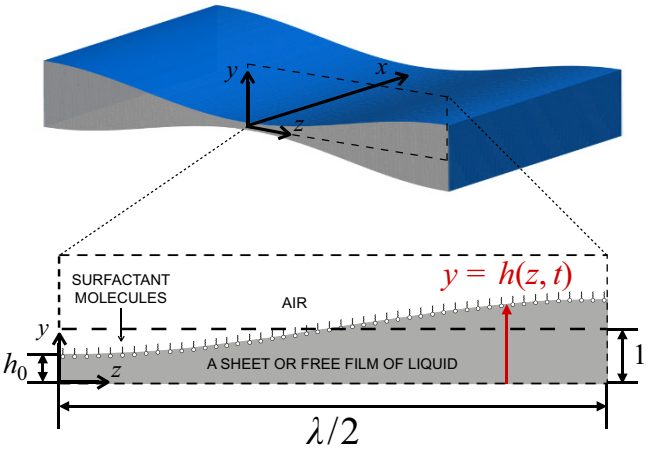

FIG. 1. A free liquid film or liquid sheet: perspective view (top) and cross-sectional view depicting the problem domain (bottom). All the variables in the figure are dimensionless so that the half-thickness of the undisturbed sheet equals unity as shown. As discussed in the text, the same variables but with tildes over them are the dimensional counterparts of those shown here.

discussion as to how surface viscous forces remain asymptotically important as rupture nears even though surfactant concentration and hence surface viscosities tend to zero as the sheet thickness tends to zero. In Sec. VII, we show how some of the results that are obtained in this paper under the assumption that surface viscosities vary linearly with surfactant concentration can be generalized for an arbitrary constitutive equation relating those variables. The paper comes to a close in Sec. VIII with concluding remarks and a brief discussion on possible directions for future studies.

II. PROBLEM FORMULATION

The system is isothermal and consists of a free film of an incompressible Newtonian fluid of constant density ρ and constant viscosity μ of unperturbed thickness $2\tilde{h}_i$ that is surrounded by a dynamically passive ambient gas that simply exerts a constant pressure, which is taken here to be the pressure datum, on the sheet (Fig. 1). The surface of the sheet—the liquid-gas (L-G) interface—is uniformly covered with a monolayer of an insoluble surfactant and the surface tension of the L-G interface when it is devoid of surfactant is given by σ_p. In this paper, we analyze the line rupture of the sheet. Thus, it proves convenient to use a Cartesian coordinate system $(\tilde{x}, \tilde{y}, \tilde{z})$ such that the $\tilde{x}$-$\tilde{z}$ plane coincides with the midplane of the undisturbed film that is parallel to and lies half way between the film's initially two flat surfaces. The $\tilde{y}$ axis emanates from the sheet's midplane and points in the direction perpendicular to the midplane. In line rupture, the dynamics is invariant, or translationally symmetric, in the $\tilde{x}$ direction.

A. Mathematical formulation: Governing equations, boundary conditions, and initial conditions

In this paper, the van der Waals-driven rupture of a surfactant-covered, quiescent liquid film is initiated by subjecting its two free surfaces at time $\tilde{t} = 0$ to shape perturbations that are symmetric with respect to the sheet's midplane. The perturbations have wavelength $\tilde{\lambda} > \tilde{\lambda}_c$ in the lateral or $\tilde{z}$ direction but are of arbitrary amplitude ε in the thin-sheet direction so that the profile of the top surface of the free film at the initial instant is given by

$$\frac{\tilde{y}(\tilde{z}, \tilde{t} = 0)}{\tilde{h}_i} = 1 - \varepsilon \cos \frac{2\pi \tilde{z}}{\tilde{\lambda}}, \tag{1}$$

Therefore, we hereafter restrict our analysis to the evolution of the sheet profile and the flow within it to the 2D domain whose lateral extent equals half of a wavelength of the imposed perturbation ($0 \leqslant \tilde{z} \leqslant \tilde{\lambda}/2$). Thus, the problem domain $\tilde{V}(\tilde{t})$ is the region bounded above by the free surface $\tilde{S}(\tilde{t})$, which is unknown a priori, bounded below by the midplane of the film located at ($\tilde{y} = 0, 0 \leqslant \tilde{z} \leqslant \tilde{\lambda}/2$), and bounded on the sides by the symmetry planes located at $\tilde{z} = 0$ and $\tilde{z} = \tilde{\lambda}/2$ as shown in Fig. 1.

The dynamics of the thinning and rupture of the sheet are analyzed by solving the transient free boundary problem consisting of the continuity and Navier-Stokes equations for fluid velocity $\tilde{\mathbf{v}} = \tilde{u}\mathbf{e}_y + \tilde{v}\mathbf{e}_z$, where $\tilde{u}$ and $\tilde{v}$ are the components of the velocity in the $\tilde{y}$ and $\tilde{z}$ directions and $\mathbf{e}_y$ and $\mathbf{e}_z$ are the unit vectors in those directions, and pressure $\tilde{p}$ within the free film $\tilde{V}(\tilde{t})$ and the convection-diffusion equation for surfactant concentration $\tilde{\Gamma}$ on $\tilde{S}(\tilde{t})$ [56]:

$$\tilde{\boldsymbol{\nabla}} \cdot \tilde{\mathbf{v}} = 0 \quad \text{in } \tilde{V}(\tilde{t}), \tag{2}$$

$$\rho\left[\frac{\partial \tilde{\mathbf{v}}}{\partial \tilde{t}} + (\tilde{\mathbf{v}} \cdot \tilde{\boldsymbol{\nabla}})\tilde{\mathbf{v}}\right] = \tilde{\boldsymbol{\nabla}} \cdot \tilde{\mathbf{T}} \quad \text{in } \tilde{V}(\tilde{t}), \tag{3}$$

$$\frac{\partial \tilde{\Gamma}}{\partial \tilde{t}} + \tilde{\boldsymbol{\nabla}}_s \cdot (\tilde{\Gamma}\tilde{\mathbf{v}}) = D_s \tilde{\nabla}_s^2 \tilde{\Gamma} \quad \text{on } \tilde{S}(\tilde{t}). \tag{4}$$

In Eq. (3), $\tilde{\mathbf{T}} = -\tilde{p}\mathbf{I} + \mu[\tilde{\boldsymbol{\nabla}}\tilde{\mathbf{v}} + (\tilde{\boldsymbol{\nabla}}\tilde{\mathbf{v}})^T]$ is the total stress tensor for a Newtonian fluid and $\mathbf{I}$ is the identity tensor. In Eq. (4), D_s is the surfactant diffusivity, $\tilde{\boldsymbol{\nabla}}_s \equiv \mathbf{I}^s \cdot \tilde{\boldsymbol{\nabla}}$ is the surface gradient operator, and $\mathbf{I}^s \equiv \mathbf{I} - \mathbf{nn}$ is the surface identity tensor with $\mathbf{n}$ denoting the outward pointing unit normal to $\tilde{S}(\tilde{t})$. As Eqs. (2) and (3) are balances of mass and momentum in the bulk $\tilde{V}(\tilde{t})$, the corresponding principles of mass and momentum conservation at the L-G interface $\tilde{S}(\tilde{t})$ are the kinematic and traction boundary conditions [57,58]. In the absence of bulk flow or mass transfer across the interface, the kinematic boundary condition is given by

$$\mathbf{n} \cdot (\tilde{\mathbf{v}} - \tilde{\mathbf{v}}_s) = 0, \tag{5}$$

where $\tilde{\mathbf{v}}_s$ is the velocity of points on the interface. In this work, the L-G interface is a compressible, two-dimensional Newtonian fluid and surface rheological effects that arise over and beyond the ordinary capillary and Marangoni stress effects are taken to be described by the Boussinesq–Scriven constitutive equation [58]. Therefore, the traction or the stress-balance boundary condition at the free-surface is given by

$$\mathbf{n} \cdot \tilde{\mathbf{T}} = 2\tilde{\mathcal{H}}\tilde{\sigma}\mathbf{n} - \frac{A_H}{6\pi(2\tilde{h})^3}\mathbf{n} + \tilde{\boldsymbol{\nabla}}_s\tilde{\sigma} + 2\tilde{\mathcal{H}}(\mu_d + \mu_s)\big(\tilde{\boldsymbol{\nabla}}_s \cdot \tilde{\mathbf{v}}\big)\mathbf{n} + \tilde{\boldsymbol{\nabla}}_s\big[(\mu_d + \mu_s)\big(\tilde{\boldsymbol{\nabla}}_s \cdot \tilde{\mathbf{v}}\big)\big]. \tag{6}$$

Here, $2\tilde{\mathcal{H}} \equiv -\tilde{\boldsymbol{\nabla}}_s \cdot \mathbf{n}$ is twice the mean curvature of the free surface the location of which is given by $\tilde{y} = \tilde{h}(\tilde{z}, \tilde{t})$ where $\tilde{h}(\tilde{z}, \tilde{t})$ is the interface shape function or the local value of the film half-thickness. In Eq. (6), $\tilde{\sigma}$ is the surface tension, and μ_s and μ_d are the surface shear and dilatational viscosities (see below). The first three terms on the right-hand side of Eq. (6) correspond to the capillary pressure, the van der Waals pressure and the Marangoni stress due to surface tension gradients. The remaining terms account for surface rheological effects.

Surface tension as well as the surface shear and the surface dilatational viscosities are all functions of surfactant concentration $\tilde{\Gamma}$, viz. $\tilde{\sigma} = \tilde{\sigma}(\tilde{\Gamma})$, $\mu_s = \mu_s(\tilde{\Gamma})$, and $\mu_d = \mu_d(\tilde{\Gamma})$. Here, surface tension $\tilde{\sigma}$ is related to surfactant concentration $\tilde{\Gamma}$ via the Szyskowsky equation of state [19,50,59]

$$\tilde{\sigma} = \sigma_p + \tilde{\Gamma}_m R_g T \ln\left(1 - \frac{\tilde{\Gamma}}{\tilde{\Gamma}_m}\right), \tag{7}$$

where $\tilde{\Gamma}_m$ is the maximum packing density of surfactant, R_g is the gas constant, and T is the absolute temperature. As opposed to the problem of jet breakup in which a cylindrical coordinate system is

the natural coordinate system used in the analysis (see, e.g., Wee *et al.* [48]), we note that here surface viscosities always appear grouped together in the form $\mu_d + \mu_s$ as a consequence of the Cartesian coordinate system used in the analysis of sheet rupture. For notational simplicity, we therefore let

$$\gamma_s \equiv \mu_d + \mu_s \tag{8}$$

and use γ_s alone in the remainder of the paper. Furthermore, as has already been stated above, we adopt a model for surface viscosity such that γ_s vanishes when $\tilde{\Gamma} = 0$. The simplest but physically realistic model for surface viscosity is that it is a linear function of $\tilde{\Gamma}$. Therefore, following recent works in the literature [47–49,60], the surface viscosity is taken to vary linearly with $\tilde{\Gamma}$ with respect to a reference state as

$$\gamma_s = \gamma_{sr}\tilde{\Gamma}/\tilde{\Gamma}_r, \tag{9}$$

where γ_{sr} is the value of the reference surface viscosity at the reference surfactant concentration $\tilde{\Gamma}_r$.

The formulation of the problem is completed by the specification of boundary conditions. These consist of symmetry conditions along the horizontal plane of symmetry located at $\tilde{y} = 0$ and the two vertical planes of symmetry located at $\tilde{z} = 0$ and $\tilde{z} = \tilde{\lambda}/2$.

B. 1D slender-sheet equations

In this section, a set of 1D long-wavelength or slender-sheet equations are derived to analyze the dynamics of sheet rupture by taking advantage of the fact that the sheet thickness is much smaller than the lateral length.

1. Characteristic scales and leading order expressions for fluid velocity and pressure

In what follows, the length scale in the $\tilde{y}$ or film thickness direction is taken to be $h_c \equiv \tilde{h}_i$, i.e., the initial film half-thickness, and the length scale in the $\tilde{z}$ or lateral direction is referred to as l_c (see below). Because of the slenderness of the sheet, $\epsilon \equiv h_c/l_c \ll 1$ where ϵ is the slenderness ratio. Thus, $|\partial\tilde{h}/\partial\tilde{z}| = O(\epsilon)$. If the scales of the velocity components in the $\tilde{y}$ and $\tilde{z}$ directions are denoted by u_c and v_c, it follows from the continuity Eq. (2) that $u_c = \epsilon v_c$ or that $u_c \ll v_c$. To determine the appropriate scales for the various components of the stress tensor and also to derive the 1D evolution equations (see below), it proves expedient to evaluate the normal and tangential components of the stress vector $\mathbf{n}\cdot\tilde{\mathbf{T}}$ at the L-G interface. These are given by

$$\mathbf{n}\cdot\tilde{\mathbf{T}}\cdot\mathbf{n} = \frac{1}{1+(\partial\tilde{h}/\partial\tilde{z})^2}\left\{\tilde{T}_{yy} - 2\frac{\partial\tilde{h}}{\partial\tilde{z}}\tilde{T}_{yz} + \left(\frac{\partial\tilde{h}}{\partial\tilde{z}}\right)^2\tilde{T}_{zz}\right\} \tag{10}$$

and

$$\mathbf{n}\cdot\tilde{\mathbf{T}}\cdot\mathbf{t} = \frac{1}{1+(\partial\tilde{h}/\partial\tilde{z})^2}\left\{\frac{\partial\tilde{h}}{\partial\tilde{z}}(\tilde{T}_{yy} - \tilde{T}_{zz}) + \left[1 - \left(\frac{\partial\tilde{h}}{\partial\tilde{z}}\right)^2\right]\tilde{T}_{yz}\right\}, \tag{11}$$

where $\mathbf{t}$ is the unit tangent to the free surface and, as usual, $\tilde{T}_{ij}$ is the ijth component of the stress tensor $\tilde{\mathbf{T}}$. The flow in a thinning slender liquid sheet is extensional in nature. For a clean interface, $\mathbf{n}\cdot\tilde{\mathbf{T}}\cdot\mathbf{t} = 0$. It then follows from Eq. (11) that the shear stress is a factor of ϵ smaller than the normal stresses or, equivalently, if the scale of the normal stresses $\tilde{T}_{zz}$ and $\tilde{T}_{yy}$ is T_c, then the scale of $\tilde{T}_{yz}$ is ϵT_c. Indeed, the relative orders of magnitude of the stress components remain unchanged when surfactants are present at the interface (see below). This is especially straightforward to appreciate from the $\tilde{z}$ component of Eq. (3) when the sheet is undergoing Stokes flow so that the left-hand side of this equation is identically zero:

$$0 = \frac{\partial\tilde{T}_{yz}}{\partial\tilde{y}} + \frac{\partial\tilde{T}_{zz}}{\partial\tilde{z}}. \tag{12}$$

Along the plane of symmetry $\tilde{y} = 0$, $\tilde{T}_{yz} = 0$. It then follows from Eq. (12) that $|\tilde{T}_{yz}| = O(\epsilon|\tilde{T}_{zz}|)$, thereby confirming that shear stress is indeed a factor of ϵ smaller than normal stress. For a Newtonian fluid, $\tilde{T}_{zz} = -\tilde{p} + 2\mu(\partial\tilde{v}/\partial\tilde{z})$ and, therefore, $T_c = \mu v_c/l_c$. Also for a Newtonian fluid, $\tilde{T}_{yz} = \mu(\partial\tilde{v}/\partial\tilde{y} + \partial\tilde{u}/\partial\tilde{z})$. Since the shear stress is a factor of ϵ times smaller than the normal stress, $\partial\tilde{v}/\partial\tilde{y} = O(\epsilon\,\partial\tilde{v}/\partial\tilde{z})$. Hence, the lateral velocity $\tilde{v}$ is asymptotically independent of the vertical coordinate $\tilde{y}$, i.e., to leading order, $\tilde{v} = \tilde{v}(\tilde{z}, \tilde{t})$. The dominant flow in the lateral direction is initiated upon the imposition of the interface perturbation at $\tilde{t} = 0$. Thus, $v_c \equiv l_c/t_c$ and the timescale t_c can be taken to be $\rho l_c^2/\mu$ when the fluid has finite density and viscosity (but see below).

We next consider the $\tilde{y}$ component of Eq. (3). With the scales introduced above, the dimensionless counterpart of that equation is given by

$$\epsilon^2\left(\frac{\partial u}{\partial t} + u\frac{\partial u}{\partial y} + v\frac{\partial u}{\partial z}\right) = \epsilon^2\frac{\partial T_{yz}}{\partial z} + \frac{\partial T_{yy}}{\partial y}, \tag{13}$$

where variables without tildes are the dimensionless counterparts of those with tildes, e.g., $\tilde{u}$ is dimensional whereas $u \equiv \tilde{u}/u_c$ is dimensionless. It follows from Eq. (13) that to leading order, T_{yy} is constant or does not vary over the cross-section of the sheet. The same conclusion also holds for T_{zz} as these two normal stresses are of the same order of magnitude. Therefore, to leading order, the pressure, in addition to the lateral velocity, is simply a function of the lateral coordinate and time, viz. $\tilde{p} = \tilde{p}(\tilde{z}, \tilde{t})$. Also to leading order, it follows from Eq. (2) that the component of the fluid velocity in the $\tilde{y}$ direction is not only much smaller than the lateral velocity $\tilde{v} = \tilde{v}(\tilde{z}, \tilde{t})$ but is given in dimensional form by $\tilde{u}(\tilde{y}, \tilde{z}, \tilde{t}) = -\tilde{y}\,(\partial\tilde{v}/\partial\tilde{z})$. In summary, the leading order expressions for the components of the fluid velocity and pressure are given by

$$\tilde{v} = \tilde{v}(\tilde{z}, \tilde{t}), \quad \tilde{u} = \tilde{u}(\tilde{y}, \tilde{z}, \tilde{t}) = -\tilde{y}\,\frac{\partial\tilde{v}}{\partial\tilde{z}}, \quad \tilde{p} = \tilde{p}(\tilde{z}, \tilde{t}). \tag{14}$$

2. 1D mass balance

If the free surface shape is represented as $\tilde{y} = \tilde{h}(\tilde{z}, \tilde{t})$ (Fig. 1), then the kinematic boundary condition can be rewritten as

$$\tilde{u} = \frac{\partial\tilde{h}}{\partial\tilde{t}} + \tilde{v}\frac{\partial\tilde{h}}{\partial\tilde{z}}. \tag{15}$$

It is noteworthy that as has already been deduced from the continuity equation, balancing of the different terms in Eq. (15) also reveals that $|\tilde{u}| = O(\epsilon|\tilde{v}|)$. Integrating the continuity Eq. (2) across the cross-section of the sheet or, equivalently, from the plane of symmetry $\tilde{y} = 0$ to the free surface $\tilde{y} = \tilde{h}$, using the symmetry boundary condition that $\tilde{u} = 0$ at $\tilde{y} = 0$, and making use of Eq. (15) reveals that

$$\frac{\partial\tilde{h}}{\partial\tilde{t}} + \frac{\partial}{\partial\tilde{z}}\int_{\tilde{y}=0}^{\tilde{y}=\tilde{h}(\tilde{z},\tilde{t})}\tilde{v}\,d\tilde{y} = 0. \tag{16}$$

However, $\tilde{v}$ is independent of $\tilde{y}$ to leading order. Therefore, Eq. (16) can be reduced to

$$\frac{\partial\tilde{h}}{\partial\tilde{t}} + \tilde{v}\frac{\partial\tilde{h}}{\partial\tilde{z}} + \tilde{h}\frac{\partial\tilde{v}}{\partial\tilde{z}} = 0. \tag{17}$$

Alternatively, Eq. (17) can also be obtained by evaluating the leading order expression for $\tilde{u}$ [see Eq. (14)] at the L-G interface, i.e., $\tilde{y} = \tilde{h}$, and substituting the result into Eq. (15). Following earlier works, Eq. (17) will henceforward be referred to as either the 1D mass balance or the kinematic boundary condition (KBC) that governs the transient evolution of the sheet half-thickness $\tilde{h}$.

3. 1D surfactant transport equation

In a quite straightforward manner, the general convection-diffusion Eq. (4) can be readily reduced to its appropriate form in the long-wavelength limit, which is henceforth referred to as

the 1D convection-diffusion (CD) equation. The appropriate equation, which governs the transient evolution of the surfactant concentration along the interface, is given by

$$\frac{\partial \tilde{\Gamma}}{\partial \tilde{t}} + \tilde{v}\frac{\partial \tilde{\Gamma}}{\partial \tilde{z}} + \tilde{\Gamma}\frac{\partial \tilde{v}}{\partial \tilde{z}} - D_s\frac{\partial^2 \tilde{\Gamma}}{\partial \tilde{z}^2} = 0. \tag{18}$$

4. 1D momentum balance

In this paper, the 1D momentum balance will be derived in a slightly different manner than the approach used by Matar [41] and Choudhury *et al.* [42] in their studies on surfactant-covered free films. The analysis is expedited by first considering the stress balance at the L-G interface at leading order. Taking the inner product of the traction boundary condition (6) with the unit tangent $\mathbf{t}$ to the interface and making use of Eq. (11), the resulting equation after nondimensionalization becomes

$$\begin{aligned}\frac{\epsilon\,\mathrm{Oh}^2}{\sqrt{1+\epsilon^2(\partial h/\partial z)^2}}&\left\{\frac{\partial h}{\partial z}(T_{yy}-T_{zz}) + \left[1-\epsilon^2\left(\frac{\partial h}{\partial z}\right)^2\right]T_{yz}\right\}\\ &= \frac{1}{\epsilon}\frac{d\sigma}{d\Gamma}\frac{\partial \Gamma}{\partial z} + \epsilon\,\mathrm{Oh}^2\frac{\partial}{\partial z}\left[B_u\frac{\frac{\partial v}{\partial z}+\epsilon^2\frac{\partial h}{\partial z}\frac{\partial u}{\partial z}}{1+\epsilon^2(\partial h/\partial z)^2}\right],\end{aligned} \tag{19}$$

where $\Gamma \equiv \tilde{\Gamma}/\tilde{\Gamma}_m$ is the dimensionless surfactant concentration and $\sigma \equiv \tilde{\sigma}/\sigma_p = 1 + \mathcal{B}^* \ln(1-\Gamma)$ is the dimensionless surface tension with $\mathcal{B}^* \equiv \tilde{\Gamma}_m R_g T/\sigma_p$ denoting the surfactant strength parameter. Here, the two dimensionless groups Oh and B_u are the Ohnesorge and Boussinesq-Scriven numbers given by

$$\mathrm{Oh} \equiv \frac{\mu}{\sqrt{\rho\sigma_p h_c}} \quad \text{and} \quad B_u \equiv \frac{\gamma_s}{\mu h_c}. \tag{20}$$

It should be noted because $\gamma_s = \gamma_s(\Gamma) = \gamma_{sr}\Gamma/\Gamma_r$ where $\Gamma_r = \tilde{\Gamma}_r/\tilde{\Gamma}_m$ is the dimensionless reference surfactant concentration, $B_u \equiv B_u(\Gamma)$ can be rewritten as

$$B_u = \frac{\gamma_s}{\mu h_c} = B_r\frac{\Gamma}{\Gamma_r} = B_0\Gamma, \tag{21}$$

where $B_r \equiv \frac{\gamma_{sr}}{\mu h_c}$ is the reference Boussinesq-Scriven number and $B_0 \equiv B_r/\Gamma_r$ is the normalized reference Boussinesq-Scriven number. We use B_r and/or B_0 in the remainder of the paper. We further note that in Eq. (19), the dimensionless surface tension gradient $\partial\sigma/\partial z$—the Marangoni stress—has been rewritten as $\partial\sigma/\partial z \equiv (d\sigma/d\Gamma)(\partial\Gamma/\partial z)$. It is important to note that Eq. (19) reveals that while the dimensional normal stresses $\tilde{T}_{yy}$ and $\tilde{T}_{zz}$ are $O(1)$ and the dimensional shear stress $\tilde{T}_{yz}$ is smaller than them by a factor of ϵ, the dimensional Marangoni stress $\partial\tilde{\sigma}/\partial\tilde{z}$ is at best of $O(\epsilon^2)$. Thus, following earlier studies on thin-sheet dynamics with Marangoni stresses induced by gradients in surfactant concentration or gradients in temperature [45,46,61], we restrict ourselves to situations where $\partial\sigma/\partial z = O(\epsilon^2)$. Equivalently, we say that $d\sigma/d\Gamma$ remains $O(\epsilon^2)$ and rescale the surfactant strength parameter so that $\mathcal{B}^* = \epsilon^2\mathcal{B}$. Therefore, keeping the highest-order contributions in Eq. (19), we conclude that the tangential stress balance at leading order is given by

$$\mathrm{Oh}^2 \mathrm{T}_{yz}|_{y=h(z,t)} = \mathrm{Oh}^2\frac{\partial h}{\partial z}(\mathrm{T}_{zz}-\mathrm{T}_{yy}) + \frac{\mathcal{B}}{\Gamma-1}\frac{\partial\Gamma}{\partial z} + \mathrm{Oh}^2\frac{\partial}{\partial z}\left(B_0\Gamma\frac{\partial v}{\partial z}\right). \tag{22}$$

Next, we take the dot or inner product of the traction boundary condition (6) with the unit normal $\mathbf{n}$ to the interface and make use of Eq. (10). The resulting equation is then nondimensionalized by using as the characteristic length in the lateral direction $l_c \equiv \sqrt{48\pi\sigma_p h_c^4/A_H}$, which arises from balancing the destabilizing van der Waals pressure driving sheet rupture with the stabilizing

capillary pressure and is of the order of the critical wavelength for linear instability, and is given by

$$\frac{\mathrm{Oh}^2}{1+\epsilon^2(\partial h/\partial z)^2}\left[T_{yy}-2\epsilon^2\frac{\partial h}{\partial z}T_{yz}+\epsilon^2\left(\frac{\partial h}{\partial z}\right)^2 T_{zz}\right]$$
$$=-\frac{1}{h^3}+\frac{\partial^2 h/\partial z^2}{[1+\epsilon^2(\partial h/\partial z)^2]^{3/2}}\left[\sigma+\mathrm{Oh}^2 B_0\Gamma\epsilon^2\frac{\epsilon^2\frac{\partial u}{\partial z}\frac{\partial h}{\partial z}+\frac{\partial v}{\partial z}}{1+\epsilon^2(\partial h/\partial z)^2}\right]. \tag{23}$$

Keeping the highest-order contributions in Eq. (23) leads to

$$\mathrm{Oh}^2\mathrm{T}_{yy}|_{y=h(z,t)}=\frac{\partial^2 h}{\partial z^2}-\frac{1}{h^3}. \tag{24}$$

As T_{yy} does not vary with y as shown earlier, Eq. (24) gives the value of the normal stress T_{yy} throughout the cross-section of the film. Comparison of Eqs. (24) and (22) makes clear that the contribution of surface viscosity to sheet thinning and rupture in the long-wavelength limit comes only from the tangential stress balance. By contrast, the effect of surface viscosity manifests itself in jet breakup through the normal stress as well as the tangential stress boundary conditions [47]. Before proceeding onto the completion of the derivation of 1D momentum equation, it is worth noting that while v, p, T_{yy}, and T_{zz} do not vary with y, T_{yz} is a function of y: it vanishes at $y=0$ because of symmetry and takes on the value given by Eq. (22) at the L-G interface.

Now that expressions have been obtained to leading order for all components of the stress tensor, the 1D force balance or the 1D momentum equation can be derived. Taking the z component of Eq. (3) at leading-order and integrating the resulting expression over the cross-section of the sheet yields

$$\frac{\partial v}{\partial t}+v\frac{\partial v}{\partial z}=\frac{1}{h}\mathrm{T}_{yz}|_{y=h(z,t)}+\frac{\partial \mathrm{T}_{zz}}{\partial z}. \tag{25}$$

When Eqs. (22) and (24) are substituted into Eq. (25), the 1D momentum equation governing the dynamics of a surfactant-covered free film is obtained:

$$\mathrm{Oh}^2\left(\frac{\partial v}{\partial t}+v\frac{\partial v}{\partial z}\right)=\frac{\partial^3 h}{\partial z^3}-\frac{\partial}{\partial z}\left(\frac{1}{h^3}\right)+\frac{\mathcal{B}}{h(\Gamma-1)}\frac{\partial\Gamma}{\partial z}$$
$$+\frac{4\mathrm{Oh}^2}{h}\frac{\partial}{\partial z}\left(h\frac{\partial v}{\partial z}\right)+\frac{\mathrm{Oh}^2}{h}\frac{\partial}{\partial z}\left(B_0\Gamma\frac{\partial v}{\partial z}\right). \tag{26}$$

The various terms in the 1D force balance correspond to the inertial force on the left-hand side of the equation and capillary force, van der Waals force, Marangoni force, bulk viscous force, and surface viscous force(s), respectively, on the right-hand side.

5. Boundary conditions for the 1D evolution equations

The 1D slender-sheet equations are solved over a lateral distance corresponding to half of a wavelength of the imposed perturbation. These evolution equations are solved subject to the boundary conditions that $\partial h/\partial z=0$, $\partial\Gamma/\partial z=0$, and $v=0$ at both ends of the 1D domain, viz. $z=0$ and $z=\lambda/2$.

III. SHEET RUPTURE FOR HIGHLY VISCOUS FLUIDS: STOKES LIMIT WHEN Pe = ∞

We first examine sheet rupture for highly viscous fluids or in the limit of Stokes flow. In this limit, $\rho=0$ or equivalently $1/\mathrm{Oh}=0$. As density cannot appear in the problem formulation in this limit, the use of the characteristic time $t_c=\rho l_c^2/\mu$ and characteristic velocity $v_c=l_c/t_c$ employed in the derivation of the long wavelength equations are no longer appropriate while the characteristic film thickness and characteristic length scale in the lateral direction, referred to here as h_{vis} and l_{vis},

remain unchanged, i.e., $h_{\text{vis}} = h_c \equiv \tilde{h}_i$ and $l_{\text{vis}} \equiv l_c = (48\pi\tilde{h}_i^4\sigma_p/A_H)^{1/2}$. Here, the proper timescale is obtained by balancing viscous and van der Waals forces and is thus given by $t_{\text{vis}} = 48\pi\tilde{h}_i^3\mu/A_H$. It is worth noting that the two characteristic times are related as $t_{\text{vis}} = t_c\text{Oh}^2$. Similarly, the characteristic velocity scale in this limit is given by $v_{\text{vis}} \equiv l_{\text{vis}}/t_{\text{vis}}$. Thus, $v_{\text{vis}} = v_c/\text{Oh}^2$. With these new time and velocity scales, Eq. (26) can be rewritten as

$$\frac{1}{\text{Oh}^2}\left(\frac{\partial v}{\partial t} + v\frac{\partial v}{\partial z}\right) = \frac{\partial^3 h}{\partial z^3} - \frac{\partial}{\partial z}\left(\frac{1}{h^3}\right) + \frac{\mathcal{B}}{h(\Gamma-1)}\frac{\partial \Gamma}{\partial z} + \frac{4}{h}\frac{\partial}{\partial z}\left(h\frac{\partial v}{\partial z}\right) + \frac{1}{h}\frac{\partial}{\partial z}\left(B_0\Gamma\frac{\partial v}{\partial z}\right). \tag{27}$$

Furthermore, we once again use the maximum packing concentration of surfactant as the characteristic surfactant concentration, viz. $\Gamma_{\text{vis}} \equiv \Gamma_c = \tilde{\Gamma}_m$. Prior to the imposition of the interface shape perturbation, the surface of the sheet is covered uniformly with surfactant at concentration $\tilde{\Gamma}_0$ or dimensionless concentration $\Gamma_0 \equiv \tilde{\Gamma}_0/\tilde{\Gamma}_m$. The dimensionless 1D evolution equations governing the dynamics of sheet thinning in the Stokes limit are then obtained by setting $1/\text{Oh}^2 = 0$ in Eq. (27) and making Eqs. (17) and (18) dimensionless with the characteristic scales that have just been introduced:

$$\frac{\partial h}{\partial t} + \frac{\partial (hv)}{\partial z} = 0, \tag{28}$$

$$\frac{\partial^3 h}{\partial z^3} - \frac{\partial}{\partial z}\left(\frac{1}{h^3}\right) + \frac{\mathcal{B}}{h(\Gamma-1)}\frac{\partial \Gamma}{\partial z} + \frac{4}{h}\frac{\partial}{\partial z}\left(h\frac{\partial v}{\partial z}\right) + \frac{1}{h}\frac{\partial}{\partial z}\left(B_0\Gamma\frac{\partial v}{\partial z}\right) = 0, \tag{29}$$

$$\frac{\partial \Gamma}{\partial t} + \frac{\partial (\Gamma v)}{\partial z} = \frac{1}{\text{Pe}}\frac{\partial^2 \Gamma}{\partial z^2}. \tag{30}$$

Here, $\text{Pe} \equiv t_D/t_{\text{vis}}$ is the Peclet number, where $t_D \equiv l_{\text{vis}}^2/D_s$ is the diffusion timescale, which denotes the relative importance of surfactant convection to diffusion. In Eq. (29) [see, also, Eqs. (9), (20), and (21)] and in the remainder of this paper, we take $\Gamma_r = \Gamma_0$ so that the reference surface viscosity $\gamma_{sr} \equiv \gamma_s|_{\tilde{\Gamma}=\tilde{\Gamma}_0}$. Therefore, the Boussinesq-Scriven number B_u is given by $B_u = B_r\Gamma/\Gamma_0$. The reader is reminded that the reference Boussinesq-Scriven number $B_r \equiv \gamma_{sr}/\mu\tilde{h}_i$ and the normalized reference Boussinesq-Scriven number $B_0 \equiv B_r/\Gamma_0$.

A. Dominant balances and similarity solutions

In this and the following section, we analyze the dynamics of sheet rupture in the limit of indefinitely large Pe, viz. when $\text{Pe} = \infty$. In such situations, surfactants are swept away from the location of the space-time singularity and are hence highly nonuniformly distributed along the L-G interface. We note that in this limit, the 1D mass balance (28) governing the time evolution of sheet half-thickness h and the 1D convection-diffusion Eq. (30) governing the time evolution of surfactant concentration Γ become identical. Hence, in this limit, surfactant concentration can be written as $\Gamma(z,t) = c(z,t)h(z,t)$. Here, the function $c(z,t)$ is governed by $Dc/Dt = 0$ where D/Dt is the 1D material time derivative. We show in the paragraph after the next one that in the vicinity of rupture, $c(z,t)$ is in fact equal to a certain constant that arises from the analysis of the governing equations in similarity space.

As the finite-time singularity (z_R, t_R) is approached, it is expected that the length and timescales of the motion in the vicinity of the rupture singularity will be orders of magnitude smaller than those in the farfield and therefore the film profile, lateral velocity and surfactant concentration can be described by similarity solutions of the form

$$h(z,t) = \tau^{\alpha_h}H(\xi), \quad v(z,t) = \tau^{\alpha_v}V(\xi),$$
$$\Gamma(z,t) = \tau^{\alpha_\Gamma}G(\xi), \quad \xi \equiv (z - z_R)/\tau^{\alpha_z}, \tag{31}$$

where $\tau = t_R - t$ is the dimensionless time to rupture, ξ is the similarity variable, α_h, α_v, α_Γ, and α_z are scaling exponents, and H, V, and G are scaling functions. Substitution of the similarity solutions (31) into the 1D mass balance (28) and enforcement that the resulting equation be independent of time or, equivalently, carrying out a kinematic balance, reveals that $\alpha_v = \alpha_z - 1$. With the use of this result, the 1D mass balance can be written as

$$\frac{H'}{H} = \frac{\alpha_h - V'}{V + \alpha_z \xi}, \tag{32}$$

where primes denote differentiation with respect to the similarity variable ξ. As a consequence of the boundedness of $V(\xi)$, there exists a point ξ_0 where the denominator on the right-hand side of Eq. (32) vanishes [38,55,62], viz. $V(\xi_0) = -\alpha_z \xi_0$. To ensure that the scaling function for the interface shape $H(\xi)$ is well behaved, the numerator on the right-hand side of this equation must also vanish at ξ_0, revealing that $V'(\xi_0) = \alpha_h$. The scaling exponent α_h can be determined from a dynamic balance which entails balancing of the dominant forces as rupture is approached. However, before doing so, we first demonstrate that the function $c(z,t)$ has to equal a constant.

Suppose that the function $c(z,t)$ is given by $c(z,t) = \tau^{\alpha_c} C(\xi)$ where α_c and $C(\xi)$ are yet another scaling exponent and another scaling function. Substitution of this expression into $Dc/Dt = 0$ yields $C'(V + \alpha_z \xi) = \alpha_c C$. Since the terms in the parenthesis in the left-hand side of this equation vanish at $\xi = \xi_0$ and $C(\xi_0) \neq 0$, it is clear that α_c must equal zero. Therefore, $C' = 0$ and hence $C(\xi) = c_0$, a constant. Thus, $c(z,t) = c_0$ and $\Gamma(z,t) = c_0 h(z,t)$. It then follows from Eq. (31) that the scaling exponents in the expressions for $h(z,t)$ and $\Gamma(z,t)$ are equal, viz. $\alpha_\Gamma = \alpha_h$. Thus, once the scaling function $H(\xi)$ is determined, the scaling function $G(\xi)$ is readily determined as $G(\xi) = c_0 H(\xi)$. Determination of c_0 will be discussed after that of the scaling exponent α_h. It is noteworthy that since $\alpha_\Gamma = \alpha_h > 0$, as the finite-time singularity is approached ($\tau \to 0$) and the thickness of the sheet tends to zero ($\alpha_h > 0$) at the location where the sheet will pinch-off, surfactant concentration must also tend to zero at that location—a realization that accords with intuition in the limit of $\mathrm{Pe} \to \infty$. Moreover, this fact allows the Marangoni stress in Eq. (29) to be rewritten as $-(\mathcal{B}/h)\partial\Gamma/\partial z$ as $\tau \to 0$ in the vicinity of the rupture point.

Now that it has been shown that $\alpha_h = \alpha_\Gamma$ and that $\alpha_v = \alpha_z - 1$, two scaling exponents, say α_h and α_z, still remain unknown. To determine the remaining unknown exponents, we substitute Eq. (31) into Eq. (29), set $G(\xi) = c_0 H(\xi)$, and carry out a dynamical balance argument between the various terms in the resulting momentum equation in similarity space:

$$0 = H'''\tau^{\alpha_h - 3\alpha_z} + \frac{4 + B_0 c_0}{H}(HV')'\tau^{\alpha_v - 2\alpha_z} + \frac{3}{H^4}H'\tau^{-3\alpha_h - \alpha_z}. \tag{33}$$

Since sheet rupture considered here is driven by attractive intermolecular van der Waals forces [38], the term that accounts for van der Waals force—the last term in Eq. (33)—is always involved in carrying out a dominant balance analysis. Thus, we first note that in arriving at Eq. (33), we have already neglected the term that accounts for Marangoni stress $(-\mathcal{B}G'/H)\tau^{-\alpha_z}$ as this term is smaller than and hence negligible compared to van der Waals force $(3H'/H^4)\tau^{-3\alpha_h - \alpha_z}$ as the finite-time singularity is approached. It is noteworthy that the surface viscous force is as important as the bulk viscous force, as revealed by each of the two contributions to the middle term in Eq. (33). Since $\alpha_v = \alpha_z - 1$, balancing van der Waals force with viscous and/or surface viscous forces yields $\alpha_h = 1/3$. Balancing van der Waals force with capillary force results in $\alpha_z = 2/3$. However, it is shown later on in this section that $\alpha_z = 0.249$ when the flow is inertialess and in the following section that $\alpha_z = 1/2$ in the presence of inertia. Hence, letting $\alpha_z = 1/2 - \varepsilon_z$ where $\varepsilon_z \geqslant 0$, it is readily seen from Eq. (33) that the capillary force varies as $\tau^{-3/2+(1/3+3\varepsilon_z)}$ whereas the other forces vary as $\tau^{-3/2+\varepsilon_z}$ as $\tau \to 0$, thereby revealing that the latter blow up at a faster rate than the former. Therefore, the dominant balance in the Stokes regime is between viscous, surface viscous and van der Waals forces while capillary force, along with the Marangoni force which has already been

shown to be unimportant, is negligible. With this realization, Eq. (33) becomes

$$0 = \frac{4 + B_0 c_0}{H}(HV')' + \frac{3}{H^4}H'. \tag{34}$$

We note that the ODEs (32) and (34) in similarity space are invariant under the transformation $\xi \to -\xi$, $H \to H$ and $V \to -V$. Results of numerical simulations of sheet thinning and rupture to be reported below reveal that the film profile is an even function and the velocity profile is an odd function with respect to $\xi = 0$ in similarity space and $z = 0$ in physical space. Thus, $\xi_0 = 0$ and $V(\xi_0) = 0$.

Since breakup is a local phenomenon, the solution far away from the rupture region should vary slowly. Therefore, in the far field in similarity space or as $|\xi| \to \infty$, the scaling functions should asymptotically vary as

$$V(\xi) \sim |\xi|^{\alpha_v/\alpha_z} = |\xi|^{1-1/\alpha_z}, \tag{35}$$

$$H(\xi) \sim |\xi|^{\alpha_h/\alpha_z} = |\xi|^{1/3\alpha_z}. \tag{36}$$

That the bulk and surface viscous forces appear together in one term in the final form of the momentum Eq. (34) in similarity space signals that it may not only prove convenient but result in great simplification if a slightly different set of scales is introduced to take advantage of this fact. Therefore, after setting $\chi \equiv (1 + B_0 c_0/4)$, we define a new characteristic timescale as $t_n \equiv \chi t_{\text{vis}}$ and a new characteristic velocity scale as $v_n \equiv l_{\text{vis}}/t_n = v_{\text{vis}}/\chi$ but retain the same values of the characeristic scales for lateral length, film thickness, and surfactant concentration. With the use of these new scales, the self-similar expressions for the dependent variables become

$$h(z,\bar{t}) = \bar{\tau}^{\alpha_h}\bar{H}(\eta), \quad \bar{v}(z,\bar{t}) = \bar{\tau}^{\alpha_v}\bar{V}(\eta), \quad \eta \equiv z/\bar{\tau}^{\alpha_z}, \tag{37}$$

where $\bar{t} \equiv \tilde{t}/t_n = t/\chi$, $\bar{v} \equiv \tilde{v}/v_n = v\chi$, $\bar{\tau} \equiv \tau/\chi$, and η is the new or rescaled similarity variable. The new scaling functions $\bar{H}(\eta)$ and $\bar{V}(\eta)$ are related to those in Eq. (31) as $\bar{H}(\eta) = H(\xi)\chi^{\alpha_h}$ and $\bar{V}(\eta) = V(\xi)\chi^{\alpha_v+1}$, respectively. Substitution of these variables into Eqs. (32) and (34) gives

$$0 = \frac{4}{\bar{H}}(\bar{H}\bar{V}')' + \frac{3}{\bar{H}^4}\bar{H}', \tag{38}$$

$$\frac{\bar{H}'}{\bar{H}} = -\frac{1/3 - \bar{V}'}{\bar{V} + \alpha_z\eta}, \tag{39}$$

where primes denote differentiation with respect to the rescaled similarity variable η. Now that the ODEs in similarity space have been rescaled, it is readily seen that the regularity condition on the new velocity scaling function requires that $\bar{V}(0) = 0$ and $\bar{V}'(0) = 1/3$. In the far field, the new scaling functions asymptotically vary as $\bar{V}(\eta) \sim |\eta|^{1-1/\alpha_z}$ and $\bar{H}(\eta) \sim |\eta|^{1/3\alpha_z}$ as $|\eta| \to \infty$. An especially noteworthy outcome of the formulation that has just been carried out by the introduction of χ and the aforementioned rescalings is that the governing ODEs (32) and (34) that account for the effects of surface viscosity due to the presence of surfactants on sheet thinning and rupture are now identical to the equations that govern the dynamics of highly viscous liquid sheets in the absence of surfactants [40]. As has already been pointed out earlier in this section and also by Thete *et al.* [40], the self-similarity that arises in this case is of the second kind and the lateral scaling exponent α_z, which cannot be inferred by kinematic and dynamic balance arguments, still needs to be determined. In their paper, Thete *et al.* [40] determined α_z by solving the 1D evolution equations numerically in physical space. Here, we use a more elegant and accurate technique that is based on a Lagrangian transformation method [63] to determine analytically the value of α_z. While doing so, we also improve slightly upon the value of α_z that was reported by Thete *et al.* [40].

B. Determination of α_z

In most studies of jet and film breakup in which the determination of similarity solutions is one of the key goals, the ODEs in similarity space are derived in terms of a similarity variable that is defined in terms of the Eulerian coordinate or independent variable z. In the approach to be used in this section, a different viewpoint is adopted where a Lagrangian variable s (defined below) is adopted and a set of ODEs is obtained in terms of the similarity variable that is based on s rather than z. In this approach, let s represent or mark a fluid area (volume per unit length in the neutral direction x in Fig. 1) in the form of a slice $\bar{h}(z,\bar{t})dz = ds$ so that instantaneous area of the sheet at any time $\bar{t}$ between two lateral locations z_1 and z_2 is given by $\int_{z_1}^{z_2} \bar{h}(z,\bar{t})\,dz = \int_{s_1}^{s_2} ds$ and let $z(s,\bar{t})$ denote the position of the area s at time $\bar{t}$. Since $\bar{h}(z,\bar{t})dz = ds$ and s marks a material object, it readily follows that that $z_s = 1/\bar{h}(z,\bar{t})$ and $z_{\bar{t}} = \bar{v}$, where subscripts denote partial differentiation with respect to those variables. Furthermore, by using the chain rule of differentiation, it is readily shown that $\partial/\partial z = z_s^{-1}\partial/\partial s$ and, moreover, that $\partial\bar{v}/\partial z = z_{s\bar{t}}/z_s$. In Lagrangian coordinates, it can be readily shown that the 1D mass balance is automatically satisfied [44]. Thus, in the new formulation, there is no counterpart of Eq. (39) in similarity space based on the Lagrangian variable s. To derive the counterpart of Eq. (38), we first need to transform the 1D momentum equation in physical space to its appropriate counterpart with respect to the Lagrangian coordinate. To make further progress, we rewrite the resulting equation in conservative form and integrate once. Upon substitution of the relations $\bar{h}(z,\bar{t}) = 1/z_s$ and $\partial\bar{v}/\partial z = z_{s\bar{t}}/z_s$ into the resulting equation, we obtain the 1D momentum balance in Lagrangian coordinates:

$$\frac{z_{s\bar{t}}}{z_s} = \frac{z_s}{4}\left[T(\bar{t}) + \frac{3}{2}z_s^2\right], \tag{40}$$

where the integration constant $T(\bar{t})$ is in fact the tension. The sheet thickness in Lagrangian coordinates is given by $\hat{H}(s,\bar{t}) = z_s^{-1}$. When this expression is used, Eq. (40) can be written as

$$\frac{\partial\hat{H}}{\partial\bar{t}} = -\frac{1}{4}\left[T(\bar{t}) + \frac{1}{\hat{H}^2}\right]. \tag{41}$$

In arriving at Eq. (41), the numerical factor of $3/2$ in Eq. (40) has been eliminated by rescaling time and the tensile force: $\bar{t} \to 2\bar{t}/3$ and $T(\bar{t}) \to 3T(\bar{t})/2$. We next note that Eq. (40) can be recast into the form

$$v_s = \frac{1}{4}\left[\frac{T}{\hat{H}^2} + \frac{1}{\hat{H}^4}\right]. \tag{42}$$

Integrating Eq. (42) from s_- to s_+, we obtain

$$T(\bar{t}) = -\frac{\int_{s_-}^{s_+}\frac{1}{\hat{H}^4}\,ds}{\int_{s_-}^{s_+}\frac{1}{\hat{H}^2}\,ds}. \tag{43}$$

Here, s_- and s_+ denote the location of boundaries far away from the rupture region at which the lateral velocity vanishes. Equation (43) shows that $T(\bar{t})$ is determined by the profile $\hat{H}(s,\bar{t})$ in a nonlocal fashion: when Eq. (41) is solved for $\hat{H}$, Eq. (43) has to be satisfied simultaneously.

To make further progress and find the local self-similar solutions of Eq. (41), we adopt the following similarity ansatz:

$$\hat{H}(s,\bar{t}) = \bar{\tau}^{\alpha_h}\psi(\xi_l), \quad T(\bar{t}) = \bar{\tau}^{\alpha_T}T_0, \quad \xi_l \equiv s/\bar{\tau}^{\alpha_\delta}, \tag{44}$$

where $\bar{\tau} = \bar{t}_R - \bar{t}$ is the dimensionless time to rupture measured in terms of t_n, ξ_l is the similarity variable based on the Lagrangian variable s, α_h, α_T, and α_δ are scaling exponents (where we have retained the symbol α_h for one of the scaling exponents), and ψ and T_0 are scaling functions. Note that because the function $T(\bar{t})$ depends only on time, its scaling function T_0 is nothing but a constant.

In writing ξ_l, we have already made use of the fact that rupture is symmetric. Since $\bar{h}(z,\bar{t})dz = ds$, the scaling exponent α_z is related to the new scaling exponents as $\alpha_z = \alpha_\delta - \alpha_h$. Inserting Eq. (44) into Eq. (41) and carrying out a dynamical balance, we obtain

$$\frac{4}{3}\psi^3(\xi_l) - 4\alpha_\delta \xi_l \psi^2(\xi_l)\psi'(\xi_l) - T_0\psi^2(\xi_l) - 1 = 0, \tag{45}$$

with $\alpha_h = 1/3$ and $\alpha_T = -2/3$. Equation (45) is an ODE for ψ but requires that we determine T_0 self-consistently. Since the profile is symmetric about the rupture point, the expansion of ψ in the vicinity of the minimum is

$$\psi(\xi_l) = \psi_0 + \xi_l^2 + \psi_2\xi_l^4 + \ldots \tag{46}$$

Here, we have used the fact that there is an arbitrary scale factor in the lateral length scale and have therefore chosen to normalize the quadratic coefficient by setting it equal to one [40]. Inserting Eq. (46) into Eq. (45), we then obtain

$$T_0 = 2\psi_0(1 - 2\alpha_\delta), \tag{47}$$

$$\psi_0^3 = \frac{3}{12\alpha_\delta - 2}. \tag{48}$$

Normalizing ψ by ψ_0, i.e., $\psi = \psi_0 f(\xi_l)$ where $f(\xi_l)$ stands for the right-hand side of Eq. (46) divided by ψ_0, and substituting Eqs. (47) and (48) into Eq. (45), we obtain

$$\frac{12\alpha_\delta f^2 df}{4f^3 - 6(1-2\alpha_\delta)f^2 + 2 - 12\alpha_\delta} = d\ln\xi_l. \tag{49}$$

Integrating Eq. (49) once and differentiating the resulting expression with respect to ξ_l, one can find $f_{\xi_l} \equiv df/d\xi_l$ in terms of $f(\xi_l)$ and α_δ. It should be noted that when the integration is carried out, an arbitrary constant of integration arises. The presence of the constant of integration in the analysis, however, does not come into play in finding α_δ. To determine α_δ, we use the constraint (43) which, in similarity variables, becomes

$$T_0\psi_0^2 = -\frac{\int_{-\infty}^{\infty}\frac{1}{f^4}\,d\xi_l}{\int_{-\infty}^{\infty}\frac{1}{f^2}\,d\xi_l}. \tag{50}$$

It is important to note that the integrals are dominated by local contributions near the singularity so that s_- and s_+ do not appear in the previous expression. To evaluate the integrals in Eq. (50), we transform the integration variable from ξ_l to f using

$$\int_{-\infty}^{\infty}\frac{1}{f^i}\,d\xi_l = 2\int_1^{\infty}\frac{1}{f_{\xi_l}f^i}\,df. \tag{51}$$

With the use of Eqs. (47) and (48), Eq. (50) becomes

$$\frac{6\alpha_\delta - 3}{6\alpha_\delta - 1} = \frac{\int_1^{\infty}\frac{1}{f_{\xi_l}f^4}\,df}{\int_1^{\infty}\frac{1}{f_{\xi_l}f^2}\,df}. \tag{52}$$

Equation (52) is a nonlinear equation for α_δ. We have solved Eq. (52) using MATLAB and have thereby determined that $\alpha_z = 0.249$ up to three decimal places. As stated earlier, the value of α_z determined in the manner that has just been outlined constitutes an improvement over the value of this exponent that was reported in Ref. [40]. Although the value of α_z determined by those authors to three decimal places was 0.256 [64], its value was reported in that publication as 0.26 after rounding off to two decimal places.

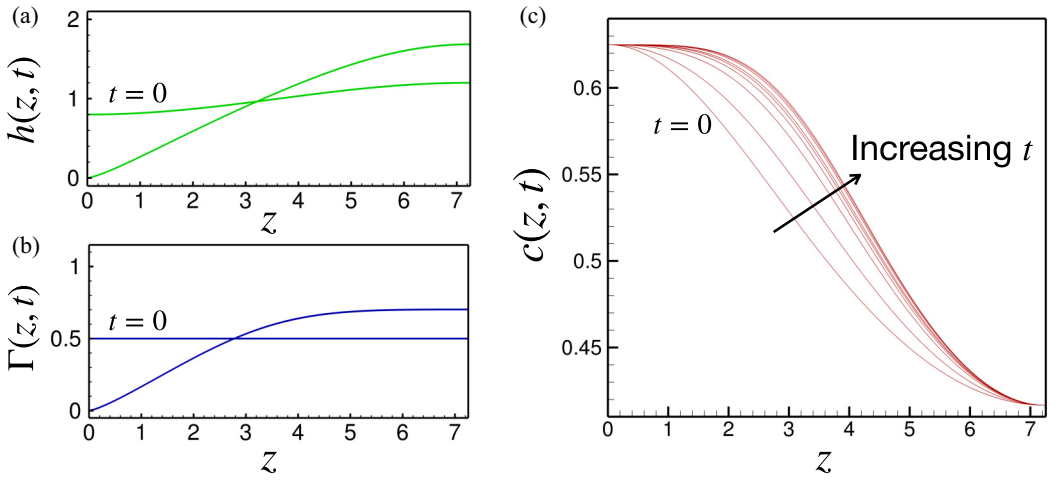

FIG. 2. Simulation results for the instantaneous profiles of the free-surface shape $h(z,t)$ and surfactant concentration $\Gamma(z,t)$ that depict the initial and late stage dynamics of a Stokes sheet, and the evolution in time of the function $c(z,t) = \Gamma(z,t)/h(z,t)$ determined from numerical solution of the evolution equations. (a) Interface shape $h(z,t)$ and (b) surfactant concentration $\Gamma(z,t)$ at the initial instant (curves marked as $t = 0$) and at the instant when $h_{\min} = 2.84 \times 10^{-4}$ (the unmarked curves). (c) Temporal evolution of the function $c(z,t) = \Gamma(z,t)/h(z,t)$ between $t = 0$ and the time when $h_{\min} = 2.84 \times 10^{-4}$. As discussed in the text, as $t \to t_R$ or $h_{\min} \to 0$, $c(z,t)$ asymptotically tends to a fixed profile that is invariant in time and, therefore, despite the entirely different initial conditions for $h(z,t)$ and $\Gamma(z,t)$, the interface shape and surfactant concentration profiles become virtually identical in form in the vicinity of the singularity as the sheet approaches rupture. Here, the reference Boussinesq-Scriven number is $B_r = 1$ (or equivalently the normalized reference Boussinesq-Scriven number $B_0 \equiv B_r/\Gamma_0 = 2$).

C. Numerical simulations

In this section, results are reported of solutions of the 1D evolution Eqs. (28)–(30) that have been obtained numerically. The evolution equations are solved subject to the boundary conditions that $\partial h/\partial z = 0$, $\partial \Gamma/\partial z = 0$, and $v = 0$ at $z = 0$ and $z = \lambda/2$, where $\lambda > \lambda_c$ (specifically, all of the simulation results that are reported in the remainder of this paper have been obtained using $\lambda = 4\lambda_c$). Whereas the initial condition on the profile of the initially quiescent film, $v(z,0) = 0$, is sinusoidal in shape [see Eq. (1)], surfactant is taken to uniformly cover the interface at the initial instant. In the simulation results to be reported in this section and also in Sec. IV, the amplitude of the disturbance to the film's surface at the initial instant $t = 0$ is taken to be $\varepsilon = 0.2$ (or, equivalently, the value of $h_0 = 0.8$—see Fig. 1) and the value of the uniform surfactant concentration at $t = 0$ is taken to be $\Gamma_0 = 0.5$.

Figure 2 shows simulation results for the evolution in time of the free-surface shape $h(z,t)$, surfactant concentration $\Gamma(z,t)$ and the function $c(z,t) = \Gamma(z,t)/h(z,t)$. Despite the entirely different initial conditions that are imposed on the free-surface shape and surfactant concentration, Figs. 2(a) and 2(b) shows that as $t \to t_R$ or $h_{\min} \to 0$, the profiles of h and Γ in the vicinity of the singularity become nearly identical in form. Therefore, their ratio, $c(z,t) = \Gamma(z,t)/h(z,t)$, becomes invariant in time in the rupture zone as shown in Fig. 2(c) and in accordance with the local theoretical analysis reported in the previous section. The evolution in time of $c(z,t)$ is dictated by $Dc/Dt = 0$. Therefore, $\partial c/\partial t = -v\partial c/\partial z$ and hence, at any instant in time, $\partial c/\partial t$ is nonnegative over the entire domain. Hence, it is expected that $c(z,t)$ should increase as time advances. However, because of symmetry, $\partial c/\partial t = 0$ at both ends of the domain. Thus, $c(0,t)$ and and $c(\lambda/2,t)$ remain invariant for all time, and hence the ratio of surfactant concentration to film half-thickness also

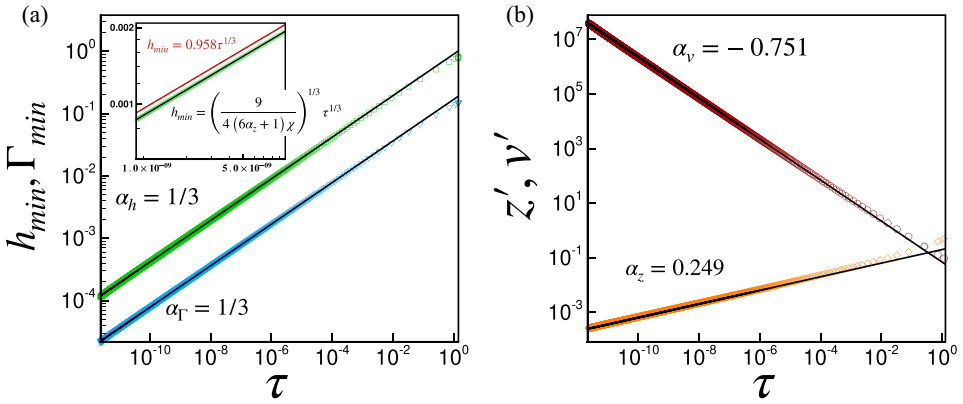

FIG. 3. Scaling behavior of key variables during rupture of liquid sheets undergoing Stokes flow: evolution in time remaining to rupture τ of the minimum sheet half-thickness $h_{\min}$ and surfactant concentration $\Gamma_{\min}$ at that location *and* lateral length z' and lateral velocity v'. The data points represent simulation results and the straight lines are the theoretical predictions. (a) Computed variation with τ of $h_{\min}$ (green square $\square$ symbols) and $\Gamma_{\min} \equiv \Gamma|_{h_{\min}}$ (blue gradient $\triangledown$ symbols). In accord with theory, the simulations predict that the scaling exponents $\alpha_h = \alpha_\Gamma = 1/3$ as indicated in the figure. Inset: Zoomed-in view of the variation of $h_{\min}$ with τ near rupture that highlights the excellent agreement between the simulations (green data points) and the theoretical predictions—the top equation in the legend [Eq. (53)] and the black line. The bottom equation in the legend and the straight red line represent the theoretical prediction for a clean interface or when surface rheological effects are absent. (b) Computed variation with τ of z' (orange diamond $\diamond$ symbols) and v' (red circle $\circ$ symbols). In accord with theory, the simulations predict that the scaling exponents for the lateral length and lateral velocity are given by $\alpha_z = 0.249$ and $\alpha_v = -0.751$ as indicated in the figure. In both this figure and the next one, the reference Boussinesq-Scriven number is $B_r = 1$ (or equivalently the normalized reference Boussinesq-Scriven number $B_0 \equiv B_r/\Gamma_0 = 2$).

remain constant and equal to their initial values for all time at these two locations. Furthermore, it follows from $Dc/Dt = 0$ that $\partial c/\partial t \approx 0$ when $v \approx 0$ or $\partial c/\partial z \approx 0$. The former holds well outside the rupture zone where the fluid is nearly stationary so that $v \approx 0$. The latter applies in the rupture zone where the value of $c(z,t)$ in the vicinity of the singularity quickly increases to $c(0, t = 0)$ due to the strong convective flow and where $\partial c/\partial z \approx 0$. Therefore, in accord with the local theoretical analysis presented in the previous section, the simulations show that as time advances and the film approaches rupture, $c(z,t)$ or the ratio of surfactant concentration to film half-thickness becomes constant, $\Gamma(z,t)/h(z,t) = \Gamma_0/h_0$, over the entire rupture zone.

Figure 3(a) shows the results obtained from 1D simulations of the variation with time remaining until rupture τ of the computed value of the minimum film half-thickness $h_{\min} \equiv h(z = 0, t)$ and surfactant concentration at that location (henceforward referred to as the minimum surfactant concentration) $\Gamma_{\min} \equiv \Gamma(z = 0, t)$. This figure makes plain that the simulation results are in excellent agreement with the scaling results predicted from theory that $h_{\min} \sim \tau^{1/3}$ and $\Gamma_{\min} \sim \tau^{1/3}$. To determine the scaling of the lateral length scale with time remaining until rupture from simulation data, the variation with τ of the z coordinate of a point located on the interface for which the film half-thickness equals a multiple of $h_{\min}$ is monitored [47,48,65]. Once again, the computed variation of the lateral scale z' with τ, which is shown in Fig. 3(b), is seen to be in excellent accord with the theoretical prediction of $z' \sim \tau^{0.249}$. The simulations further show [Fig. 3(b)] that the variation with τ of the lateral velocity v' calculated at z' is also in excellent agreement with the scaling result predicted from theory that $v' \sim \tau^{-0.751}$.

A result of perhaps greatest utility to experimentalists is the variation with time of the minimum value of the half-thickness of the thinning sheet. The minimum sheet half-thickness $h_{\min}$ can be

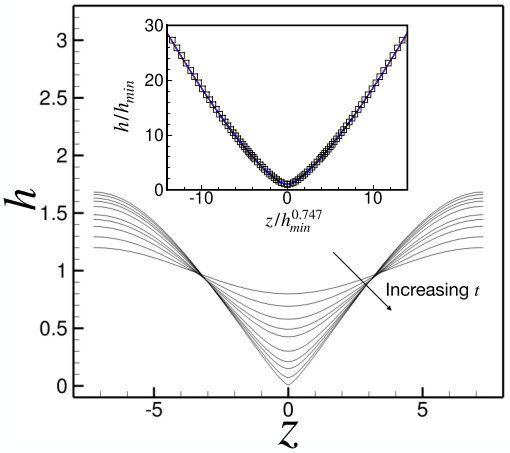

FIG. 4. Evolution in time of the free-surface profile and self-similarity of the interface shape during rupture of sheets undergoing Stokes flow. The main figure shows the film profile $h(z, t)$ determined from simulations at ten instances in time and confirms that sheet rupture is symmetric as predicted from theory. Inset: appropriately rescaled interface shapes obtained from solution of the transient partial differential evolution equations in physical space (curves) agree well with the normalized similarity profile obtained from solution of the ODEs in similarity space (symbols). The individual curves obtained from the simulations are hard to distinguish from one another because of the excellence of the collapse and/or the closeness of the collapsed solutions to one another.

calculated from Eq. (48) after recalling that $\hat{\tau} = 3\tau/2\chi$ and $\alpha_\delta = \alpha_z + \alpha_h$:

$$h_{\min} = \psi_0 \hat{\tau}^{1/3} = \left[\frac{9}{4(6\alpha_z + 1)\chi}\right]^{1/3} \tau^{1/3}. \tag{53}$$

The inset to Fig. 3(a) shows that both the scaling with τ of $h_{\min}$ and the value of the prefactor in the theoretical result (53) are in excellent agreement with the scaling with τ and the prefactor of $h_{\min}$ obtained from the numerical solution of the transient system of 1D partial differential evolution equations. Here, the red solid line is the solution reported by Thete *et al.* [40], $h_{\min} = 0.958\tau^{1/3}$, for a sheet with a clean interface or a surfactant-covered sheet in the absence of surface rheological effects. We note that as the Boussinesq-Scriven number $B_u \to 0$, $\chi \to 1$ and Eq. (53) reduces to $h_{\min} = 0.966\tau^{1/3}$, which is in excellent agreement with the solution reported by Thete *et al.* [40]—both analyses show that $h_{\min} \sim \tau^{1/3}$—but improves slightly upon the value of the prefactor of 0.958 reported by them.

To demonstrate the self-similarity of the interface profiles, it is instructive to plot together the scaling function $H(\xi)$ from theory and appropriately collapsed film profiles obtained from the solution of the evolution equations. The scaling function $H(\xi)$ determined from theory can be used to express the similarity solution for the interface profile in normalized form as $h/h_{\min} = H(\xi)/H(0)$. Similarly, instantaneous interface shape profiles obtained from the solution of the transient PDEs (Fig. 4) can be normalized as $h/h_{\min} = h(z, t)/h(0, t)$. Moreover, since $\xi = z/[h_{\min}/H(0)]^{\alpha_z/\alpha_h}$, rather than plotting the normalized interface shapes as a function of ξ, it is more convenient to plot $h/h_{\min}$ as a function of $z/h_{\min}^{0.747}$ where $\alpha_z/\alpha_h = 0.249/(1/3) = 0.747$. The inset to Fig. 4 shows that transient profiles obtained from the solution of the transient PDEs in physical space when collapsed in the manner just described tend as $t \to t_R$ or $h_{\min} \to 0$ to the self-similar profile predicted from the solution of the ODEs in similarity space.

D. Validity of the long-wavelength or slenderness approximation in Stokes flow

In the Stokes limit, the local slope $\partial h/\partial z$ varies with time to rupture τ as $\tau^{\alpha_h-\alpha_z} = \tau^{1/3-0.249} = \tau^{0.0843}$. Thus, the sheet becomes locally more slender as $\tau \to 0$ and approaches rupture.

E. Asymptotic validity of the neglect of inertia

When $\mathrm{Oh} \gg 1$, the thinning and rupture of liquid sheets are expected to follow the Stokes scaling laws that have been obtained in this section. According to Eq. (27), when $\mathrm{Oh} \gg 1$, the dominant forces—van der Waals, bulk viscous and surface viscous forces—all scale as $\tau^{-\alpha_z-1}$ as the sheet thins. If, however, one then estimates the variation with time remaining to rupture of the inertial terms which are set equal to zero in the Stokes limit, it is found that both of these terms scale as $\tau^{\alpha_z-2}/\mathrm{Oh}^2$. Therefore, the inertial terms, which are neglected in the analysis of the Stokes limit, blow up at a faster rate than the forces that enter the dominant balance of forces in that limit when Oh is large but not infinite. Thus, as $\tau \to 0$, it is expected that inertia would catch up to the van der Waals, bulk viscous and surface viscous forces. Therefore, the neglect of inertia is asymptotically inconsistent and the Stokes regime is only an initial or transitory regime when $\mathrm{Oh} \gg 1$.

The time and/or the value of the minimum sheet half-thickness when this transition occurs can be estimated by balancing the inertial terms with the terms corresponding to the van der Waals, bulk viscous and surface viscous forces, viz.

$$\frac{1}{\mathrm{Oh}^2}\tau^{\alpha_z-2} \approx \tau^{-\alpha_z-1}. \tag{54}$$

Thus, the transition from the Stokes regime to an inertial-viscous regime (to be analyzed in the next section) where inertia is no longer negligible can be estimated to occur when

$$\tau \approx \mathrm{Oh}^{\frac{2}{2\alpha_z-1}}. \tag{55}$$

However, since $h_{\min} \sim \tau^{1/3}$, the minimum value of the film half-thickness at which the transition occurs can be estimated to be

$$h_{\min} \approx \mathrm{Oh}^{\frac{2/3}{2\alpha_z-1}} \approx \mathrm{Oh}^{-1.328}. \tag{56}$$

Thus, when $\mathrm{Oh} = 10^3$, the transition would occur when $h_{\min} \approx 10^{-4}$. Hence, if the dimensional initial film half-thickness is 1 μm, the transition is expected to occur when $\tilde{h}_{\min}$ has fallen to 0.1 nm. Since this value is well below the continuum limit of 10 nm, the dynamics is expected to remain in the Stokes regime during the entire period of thinning. If, however, $\mathrm{Oh} = 10$, then the transition should occur when $h_{\min} \approx 0.04$. For a film of the same initial thickness, the transition would then occur when $\tilde{h}_{\min} \approx 40$ nm and should be observable in the laboratory.

IV. SHEET RUPTURE WITH INERTIA WHEN Pe = ∞

In this section, we first properly nondimensionlize the evolution equations governing sheet rupture when inertia is no longer negligible. We then carry out a local theoretical analysis of sheet thinning and rupture, and conclude the section by presenting numerical solutions of the evolution equations. For slightly viscous sheets, the appropriate timescale is that which is obtained from a capillary–van der Waals balance. Hence, instead of taking $t_c = \rho l_c^2/\mu$, we take the new timescale to be $t_{\mathrm{cap}} = (\rho l_{\mathrm{cap}}^4/\sigma_p \tilde{h}_i)^{1/2}$ but retain the same choice for lateral length as before so that $l_{\mathrm{cap}} = l_c$. Thus, $t_{\mathrm{cap}} = t_c\mathrm{Oh}$. With these two scales, the new velocity scale is $v_{\mathrm{cap}} = l_{\mathrm{cap}}/t_{\mathrm{cap}} = v_c/\mathrm{Oh}$. Upon the introduction of these new time and velocity scales, Eq. (26) can be rewritten as

$$\frac{\partial v}{\partial t} + v\frac{\partial v}{\partial z} = \frac{\partial^3 h}{\partial z^3} - \frac{\partial}{\partial z}\left(\frac{1}{h^3}\right) + \frac{\mathcal{B}}{h(\Gamma-1)}\frac{\partial \Gamma}{\partial z} + \frac{4\mathrm{Oh}}{h}\frac{\partial}{\partial z}\left(h\frac{\partial v}{\partial z}\right) + \frac{\mathrm{Oh}}{h}\frac{\partial}{\partial z}\left(B_0\Gamma\frac{\partial v}{\partial z}\right). \tag{57}$$

Although the characteristic time and velocity scales are now different from those for Stokes flow, the dimensionless KBC and CD equations remain unchanged when $\mathrm{Pe} \to \infty$, and hence are given by

$$\frac{\partial h}{\partial t} + \frac{\partial (hv)}{\partial z} = 0, \tag{58}$$

$$\frac{\partial \Gamma}{\partial t} + \frac{\partial (\Gamma v)}{\partial z} = 0. \tag{59}$$

A. Dominant balances and similarity solutions

In the absence of surfactants, Vaynblat *et al.* [38] have shown that as rupture is approached, sheets with clean interfaces asymptotically thin according to

$$\frac{\tilde{h}_{\min}}{\tilde{h}_i} = 0.7401 \left(\frac{\tilde{\tau}}{t_\mu} \right)^{1/3}, \tag{60}$$

where $t_\mu \equiv \rho l_\mu^2/\mu$ and $l_\mu = (48\pi \tilde{h}_i^3 \mu^2/\rho A_H)^{1/2}$. The characteristic scales in Eq. (60) are intimately tied to the dynamical balance between the three forces at play: van der Waals, inertia, and bulk viscous forces. Here, the power-law exponent of $1/3$ that determines how the minimum half-thickness scales with time remaining until rupture, viz. $\tilde{h}_{\min} \sim \tilde{\tau}^{1/3}$, and the amplitude or coefficient of 0.7401 in the nondimensional scaling law (60) are universal. Remarkably, when surfactants are present but surface rheological effects are neglected and diffusion is sufficiently weak, the same balance of forces is observed to hold during sheet thinning [41,42]. To date, however, neither a self-similar analysis predicting this thinning rate has been carried out nor an expression analogous to Eq. (60) for surfactant concentration has been obtained. In the next few paragraphs, we remedy this situation by providing such analyses in both the absence and presence of surface rheological effects.

Following Vaynblat *et al.* [38], we measure the sheet half-thickness $\tilde{h}$, the lateral velocity $\tilde{v}$ and the lateral length $\tilde{z}$ in units of $\tilde{h}_i$, l_μ/t_μ, and l_μ and adopt the following similarity ansatz:

$$h(z,t) = \tau^{1/3} H(\xi), \quad v(z,t) = \tau^{-1/2} V(\xi), \quad \xi \equiv z/\tau^{1/2}, \tag{61}$$

Vaynblat *et al.* [38] have already shown that the governing ODEs in similarity space for a Newtonian sheet with a clean interface are given by

$$\frac{1}{2}V + \frac{\xi}{2}V' + VV' = \frac{4}{H}(HV')' + \frac{3}{H^4}H', \tag{62}$$

$$\frac{H'}{H} = -\frac{1/3 - V'}{V + \alpha_z \eta}, \tag{63}$$

subject to the far field conditions that

$$V(\xi) \sim \xi^{\alpha_v/\alpha_z} = \xi^{-1}, \tag{64}$$

$$H(\xi) \sim \xi^{\alpha_h/\alpha_z} = \xi^{2/3}, \tag{65}$$

as $|\xi| \to \infty$. It is noteworthy that the universal scaling exponents $\alpha_h = 1/3$, $\alpha_v = -1/2$, and $\alpha_z = 1/2$ result as a consequence of balance of forces between inertial, van der Waals and bulk viscous forces. If one were to perform the same analysis for a Newtonian sheet using the different characteristic scales $\tilde{h}_i$, l_c, and t_{cap}, one would obtain almost the same albeit slightly altered set of governing ODEs, scaling exponents and far field conditions such that Oh would now appear in front of the term that accounts for the bulk viscous force.

For surfactant-covered Newtonian sheets in the absence of surface rheological effects in the limit that $\mathrm{Pe} \to \infty$, the same scaling exponents result as a consequence of the balance of the three aforementioned forces and the insignificance of Marangoni force as the sheet tends toward breakup [41]. In other words, the ODEs that arise from the momentum and mass balances in similarity space

remain unchanged when surfactants are present because the 1D momentum equation is decoupled from the 1D CD equation [48] as a consequence of the Marangoni stress being subdominant in the limit when surfactants are convected away from the rupture zone (Pe $\to \infty$). Therefore, in this limit, $\Gamma = c_0 h$, and the scaling function for Γ in similarity space is linearly proportional to $H(\xi)$ via the proportionality constant c_0. Hence, it is not necessary to solve for Γ in similarity space. Since the governing ODEs are the same with or without surfactants, the thinning rate in the presence of surfactants must be the same as that given by Eq. (62). When account is taken of the difference in characteristic timescales used here and by Vaynblat *et al.* [38], viz. $t_{\rm cap}$ or t_μ such that $t_\mu = {\rm Oh}\, t_{\rm cap}$, Eq. (60) can be rewritten as follows when $\tilde{t}$ has been nondimensionalized by $t_{\rm cap}$:

$$h_{\rm min} = \frac{0.7401}{{\rm Oh}^{1/3}} \tau^{1/3}. \tag{66}$$

When surface rheological effects are present, the aforementioned decoupling in similarity space between the 1D momentum and the 1D CD equations does not occur, thereby necessitating a more involved analysis for determining the counterpart of Eq. (66) which takes proper account of surface rheolgoical effects. However, such a complicated analysis can once again be avoided in the limit that Pe $\to \infty$. Here, we remind the reader that surface rheological effects are accounted for by a single additional term in the 1D momentum balance equation and that this term can be combined with its bulk counterpart in similarity space by the introduction of the parameter χ, which represents the importance of bulk viscous force to its surface counterpart, into the definition of the characteristic timescale [see the transformation of Eq. (34) into Eq. (38)]. Thus, surface rheological effects are just as important as their bulk counterparts when Pe $\to \infty$ and inertia is not negligible. We note that Marangoni stresses are once again subdominant in this limit due to the dominance of convection, which tends to evacuate surfactant out of the rupture zone, over diffusion. In summary, surface viscosity brings about a new dynamical regime in which inertial, van der Waals, bulk viscous and surface viscous forces are in balance and the scaling exponents are unaltered compared to those in the absence of surface rheological effects.

As the details of the approach have already been laid out in the Stokes flow analysis presented earlier, we shall simply summarize here how the parameter χ is used in the derivation of the expression of the thinning rate. By using as characteristic timescale $t_n \equiv {\rm Oh}\, t_{\rm cap}\, \chi$ instead of $t_{\rm cap}$, it is straightforward to show that the governing ODEs, scaling exponents and far field conditions are identical to Eqs. (62)–(65) in similarity space when inertia cannot be neglected. Thus, after exploiting the similarities between the analysis of sheets undergoing Stokes flow and that of sheets undergoing inertial-viscous flow and with the appreciation of the competitive interplay between bulk viscous force and its surface counterpart, the rate of thinning of a surfactant-covered sheet in the presence of surface rheological effects can be shown to be given by

$$h_{\rm min} = \frac{0.7401}{{\rm Oh}^{1/3} \chi^{1/3}} \tau^{1/3}. \tag{67}$$

We note that as the Boussinesq-Scriven number $B_u \to 0$, $\chi \to 1$ and Eq. (67) reduces to Eq. (66).

B. Numerical simulations

In this section, results are presented of solutions of the 1D evolution Eqs. (58) and (59) that have been obtained by simulation. The approach follows that which has already been summarized in the analysis of thinning of liquid sheets undergoing Stokes flow.

Figure 5(a) shows the results obtained from 1D simulations of the variation with time remaining until rupture τ of the computed value of the minimum film half-thickness $h_{\rm min}$ and surfactant concentration at that location $\Gamma_{\rm min}$. This figure makes plain that the simulation results are in excellent agreement with the scaling results predicted from theory that $h_{\rm min} \sim \tau^{1/3}$ and $\Gamma_{\rm min} \sim \tau^{1/3}$. The scaling of the lateral length is determined in the same manner as that described earlier in Sec. III C. Once again, the computed variation of the lateral length z' with τ is seen to be in excellent accord

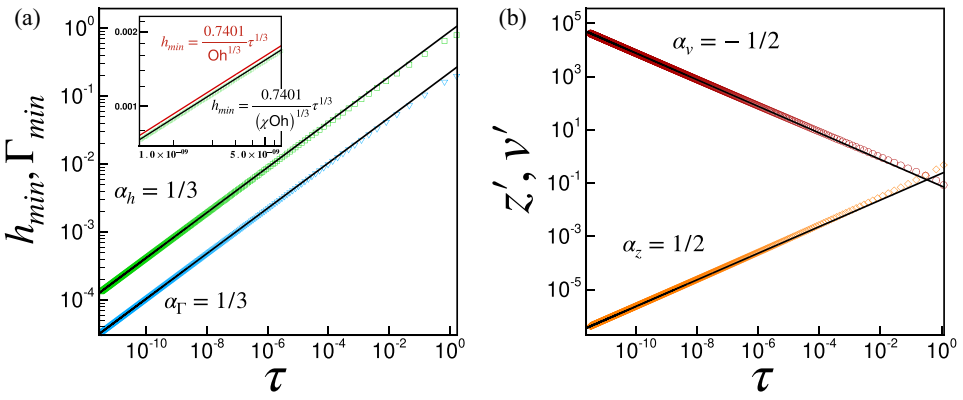

FIG. 5. Scaling behavior of the minimum sheet half-thickness $h_{\min}$, surfactant concentration $\Gamma_{\min}$ at that location, lateral length z', and lateral velocity v' during rupture of liquid sheets undergoing inertial-viscous flow or when inertia is not negligible: evolution in time remaining to rupture τ of $h_{\min}$, $\Gamma_{\min}$, z', and v'. The data points represent simulation results and the straight lines are the theoretical predictions. (a) Simulation results for the computed variation with τ of $h_{\min}$ (green square $\square$ symbols) and $\Gamma_{\min} \equiv \Gamma|_{h_{\min}}$ (blue gradient $\triangledown$ symbols). The simulations predict that the scaling exponents $\alpha_h = \alpha_\Gamma = 1/3$, in accord with theory and as indicated in the figure. Inset: Zoomed-in view of the variation of $h_{\min}$ with τ near rupture that highlights the excellent agreement between the simulations (green data points) and the theoretical predictions—the top equation in the legend [Eq. (67)] and the black line. The bottom equation in the legend and the straight red line represent the theoretical prediction [Eq. (66)] for a clean interface or when surface rheological effects are absent. (b) Computed variation with τ of z' (orange diamond $\diamond$ symbols) and v' (red circle $\circ$ symbols). The simulations predict that the scaling exponents for the lateral length and lateral velocity are given by $\alpha_z = 1/2$ and $\alpha_v = -1/2$, in accord with theory and as indicated in the figure. Here, the Ohnesorge number $\mathrm{Oh} = 0.5$ and the reference Boussinesq-Scriven number is $B_r = 2$ (or equivalently the normalized reference Boussinesq-Scriven number $B_0 \equiv B_r/\Gamma_0 = 4$).

with the theoretical prediction of $z' \sim \tau^{1/2}$ as shown in Fig. 5(b). The simulations further show [Fig. 5(b)] that the variation with τ of the lateral velocity v' calculated at z' is also in excellent agreement with the scaling result predicted from theory that $v' \sim \tau^{-1/2}$.

The inset to Fig. 5(a) shows that both the scaling with τ of $h_{\min}$ and the value of the prefactor in the theoretical result (67) (denoted by the black line) are in excellent agreement with the scaling with τ and the prefactor of $h_{\min}$ obtained from the numerical solution of the transient system of 1D partial differential evolution equations. The inset also shows for comparison the corresponding solution for a sheet with a clean interface or a surfactant-covered sheet in the absence of surface rheological effects ($\chi = 1$, denoted by the red line).

To demonstrate the self-similarity of the interface profiles, the normalized scaling function $h/h_{\min} = H(\xi)/H(0)$ is plotted together with the appropriately collapsed film profiles $h/h_{\min} = h(z,t)/h(0,t)$ as shown in figure 6. Since $\xi = z/(h_{\min}/H(0))^{\alpha_z/\alpha_h}$, the scaled profiles are plotted as a function of $z/h_{\min}^{1.5}$. Figure 6 makes plain that the interface profiles obtained from the solution of the governing transient PDEs are in excellent agreement with the normalized similarity profile obtained from the solution of the ODEs in similarity space.

C. Validity of the long-wavelength approximation in inertial-viscous flow

When inertia is not negligible, the local slope $\partial h/\partial z$ of the interface varies with time to rupture τ as $\tau^{\alpha_h - \alpha_z} = \tau^{1/3-1/2} = \tau^{-1/6}$. Therefore, the local slope diverges as $\tau \to 0$ and would become of order one no matter how small its initial value. However, the long-wavelength approximation would be valid for all time if molecular length scales are reached before the interface slope becomes of O(1).

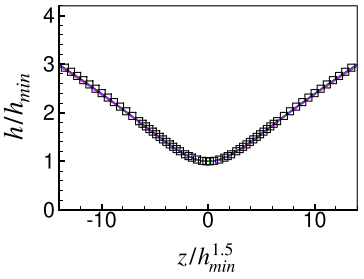

FIG. 6. Self-similarity of the interface shape during rupture of sheets undergoing inertial-viscous flow. Appropriately rescaled interface shapes obtained from solution of the transient partial differential evolution equations in physical space (curves) agree well with the normalized similarity profile obtained from solution of the ODEs in similarity space (symbols). The individual curves obtained from the simulations are hard to distinguish from one another because of the excellence of the collapse and/or the closeness of the collapsed solutions to one another. Here, the Ohnesorge number Oh = 0.5 and the reference Boussinesq-Scriven number is $B_r = 4$ (or equivalently the normalized reference Boussinesq-Scriven number $B_0 \equiv B_r/\Gamma_0 = 8$.)

Initially, the sheet is slender and the initial value of the slenderness ratio Λ is given by

$$\Lambda|_{t=0} \equiv \epsilon = \frac{\tilde{h}_i}{l_c} \approx \frac{\tilde{h}_i}{\tilde{h}_i^2/d} = \frac{d}{\tilde{h}_i} \ll 1. \tag{68}$$

The reader is reminded that the molecular length scale d is of the order a nanometer and the initial film half-thickness is of the order of a micrometer. Since the dimensional sheet half-thickness scales as $\tilde{h}_i\tau^{1/3}$ and the dimensional lateral extent of the rupture zone scales as $l_c\tau^{1/2}$, the instantaneous value of the slenderness ratio Λ scales as

$$\Lambda \sim \frac{\tilde{h}_i\tau^{1/3}}{l_c\tau^{1/2}} \approx \frac{d}{\tilde{h}_i}\tau^{-1/6} \approx \epsilon\tau^{-1/6}. \tag{69}$$

The slenderness ratio becomes of O(1) when $\epsilon\tau^{-1/6} \approx 1$. Since $h \sim \tau^{1/3}$, the minimum value of the dimensionless sheet half-thickness when this happens is given by $h_{\min} \approx \epsilon^2$. Therefore, the slenderness ratio becomes O(1) when the dimensional values of the film half-thickness and the lateral length scale are of the order of $\tilde{h}_i\epsilon^2 \approx d^2/\tilde{h}_i \equiv d(d/\tilde{h}_i) \ll d$. Thus, the continuum assumption breaks down well before the long-wavelength assumption does.

V. SHEET THINNING AND RUPTURE AT LARGE BUT FINITE PECLET NUMBER

So far in this paper, we have only considered sheet thinning when Pe = ∞. In this section, we consider the effect of large but finite Pe on sheet thinning and rupture.

To understand the effect of finite Pe on the dynamics, we examine the CD equation in nondimensional form:

$$\frac{\partial\Gamma}{\partial t} + \frac{\partial(\Gamma v)}{\partial z} = \frac{1}{\mathrm{Pe}}\frac{\partial^2\Gamma}{\partial z^2}. \tag{70}$$

Here, we have used the same characteristic scales to nondimensionalize surfactant concentration $\tilde{\Gamma}$ and lateral length $\tilde{z}$, viz. $\Gamma \equiv \tilde{\Gamma}/\tilde{\Gamma}_m$ and $z \equiv \tilde{z}/l_c$. We have nondimensionalized time $\tilde{t}$ as $t \equiv \tilde{t}/t_*$ where the characteristic time t_* is t_{vis} in the Stokes limit and t_{cap} in inertial-viscous flow. In both cases, we have defined the characteristic velocity as $v_* \equiv l_c/t_*$. The Peclet number in the two cases is given by $\mathrm{Pe} \equiv l_c^2/D_s t_*$.

Once again, we take that as the finite-time singularity (z_R, t_R) is approached, the length and timescales of the motion in the vicinity of the rupture singularity will be orders of magnitude smaller than those in the farfield and therefore the film profile, lateral velocity, and surfactant concentration

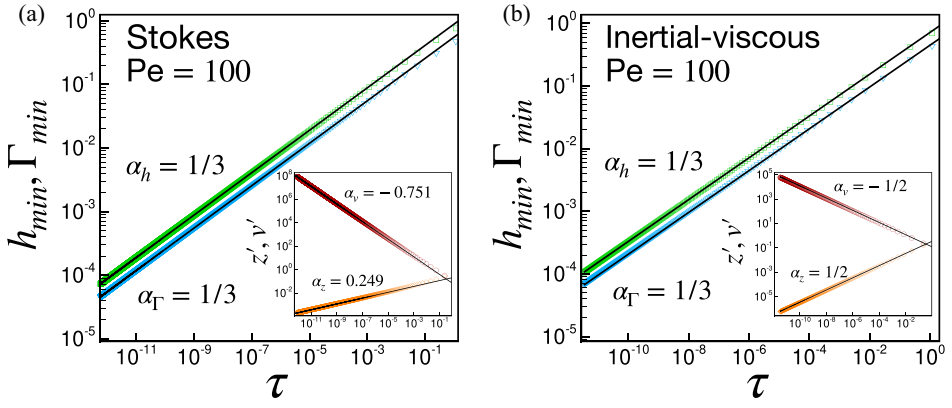

FIG. 7. Scaling behavior of the minimum sheet half-thickness $h_{\min}$, surfactant concentration $\Gamma_{\min}$ at that location, lateral length z', and lateral velocity v' during rupture of liquid sheets undergoing (a) Stokes flow and (b) inertial-viscous flow at large but finite Peclet number $\mathrm{Pe} = 100$: evolution in time remaining to rupture τ of $h_{\min}$ and $\Gamma_{\min}$ (main figures) and of z' and v' (insets). The data points represent simulation results and the straight lines are the theoretical predictions when $\mathrm{Pe} = \infty$. Main figures: simulation results for the computed variation with τ of $h_{\min}$ (green square $\square$ symbols) and $\Gamma_{\min} \equiv \Gamma|_{h_{\min}}$ (blue gradient $\triangledown$ symbols). The simulations predict that the scaling exponents $\alpha_h = \alpha_\Gamma = 1/3$, in accord with theoretical and simulation results when $\mathrm{Pe} = \infty$ and as indicated in the figure. Insets: simulation results for the computed variation with τ of z' (orange diamond $\diamond$ symbols) and v' (red circle $\circ$ symbols). The simulations predict that the scaling exponents $\alpha_z = 0.249$ and $\alpha_v = -0.751$ in Stokes flow and $\alpha_z = 1/2$ and $\alpha_v = -1/2$ in inertial-viscous flow, also in accord with theoretical and simulation results when $\mathrm{Pe} = \infty$ and as indicated in the figure. In panel (a), the reference Boussinesq-Scriven number is $B_r = 1$ (or equivalently $B_0 \equiv B_r/\Gamma_0 = 2$). In panel (b), the Ohnesorge number $\mathrm{Oh} = 0.5$ and the reference Boussinesq-Scriven number is $B_r = 4$ (or equivalently the normalized reference Boussinesq-Scriven number $B_0 \equiv B_r/\Gamma_0 = 8$).

can be described by similarity solutions of the form given by Eq. (31). In similarity space, Eq. (70) can be written as

$$\alpha_z \xi G' - \alpha_\Gamma G + (GV)' = \frac{\tau^{1-2\alpha_z}}{\mathrm{Pe}} G'', \tag{71}$$

where we have made use of the fact that the kinematic balance once again reveals that the scaling exponents α_v and α_z are related as $\alpha_v = \alpha_z - 1$. In Eq. (71), the relative importance of diffusion compared to convection is given by the prefactor $\tau^{1-2\alpha_z}/\mathrm{Pe}$ multiplying G''. In Secs. III and IV where $\mathrm{Pe} = \infty$, the right-hand side of Eq. (71) is exactly zero and diffusion is negligible compared to convection during the entire period of sheet thinning. The physics, however, is more complex when $0 < \mathrm{Pe} < \infty$.

When Pe is finite but nonzero, it follows from Eq. (71) that diffusion is unimportant as $\tau \to 0$ if $\alpha_z < 1/2$. More precisely, diffusion becomes negligible compared to convection when $\tau < \mathrm{Pe}^{1/(1-2\alpha_z)}$. Therefore, for a liquid undergoing Stokes flow, if the value of the lateral scaling exponent α_z when $\mathrm{Pe} \neq \infty$ remains unchanged compared to when $\mathrm{Pe} = \infty$ or has some other value that is nevertheless less than $1/2$, diffusion will be asymptotically negligible compared to convection as the sheet tends toward rupture. According to Eq. (71), if $\alpha_z = 1/2$, then the relative importance of diffusion to convection remains unchanged as the sheet thins. Therefore, for a liquid undergoing inertial-viscous flow, if the value of the lateral scaling exponent α_z when $\mathrm{Pe} \gg 1$ but not infinite remains unchanged compared to when $\mathrm{Pe} = \infty$, then diffusion should be negligible compared to convection during the entire period of thinning.

Figure 7 shows results obtained from the numerical solution of the 1D evolution equations—Eqs. (28), (29), and (70) for a sheet undergoing Stokes flow ($\mathrm{Oh} = \infty$) and Eqs. (58), (59), and

(70) for a sheet undergoing inertial-viscous flow (Oh = 0.5)—when Pe = 100. The main parts of Figs. 7(a) and 7(b) show the results obtained from 1D simulations of the variation with time remaining until rupture τ of the computed value of the minimum film half-thickness $h_{\min}$ and surfactant concentration at that location $\Gamma_{\min}$. The inserts in both parts (a) and (b) of this figure show the variation with τ of the lateral length z' and the lateral velocity v'. According to the results that are depicted in Fig. 7, the values of the scaling exponents when Pe = 100 are identical to those obtained earlier from theory and simulations when Pe = ∞ regardless of whether inertia is negligible or inertia cannot be neglected.

VI. WHY SURFACE VISCOSITIES AND SURFACE VISCOUS STRESSES ARE IMPORTANT EVEN WHEN SURFACTANTS ARE SWEPT AWAY FROM THE RUPTURE ZONE

According to the foregoing results, surfactants are swept out of the rupture zone and surfactant concentration tends to zero as sheet thickness approaches zero when Pe $\gg 1$. Therefore, it is remarkable but counterintuitive that surface viscosities can be important even when surfactants are swept away from the rupture zone and, consequently, surface viscosities vanish. A simple explanation of this interesting result lies in the competition between two effects. A differential section of axial length dz of a slender sheet has volume per unit length in the neutral direction $dV = 2h\,dz$ and interfacial area per unit length in the neutral direction $dA = 2\,dz$ (the factors of two account for the presence of the two halves and two free surfaces of the sheet). Thus, surface area to volume ratio scales as $1/h$ and increases without bound as the sheet thickness tends to zero ($h \to 0$). Moreover, it follows from the 1D momentum equation that the ratio of surface viscous to bulk viscous force scales as $B_0\Gamma/4h$. When Pe = ∞, $h \sim \Gamma$. Thus, surface viscous stress can remain comparable to bulk viscous stress even as surfactants are swept away from the rupture zone and surface viscosities are tending to zero because surface area-to-volume ratio $1/h \to \infty$ as $h \to 0$.

VII. GENERAL CONSTITUTIVE RELATION FOR γ_s

Although the use of a specific constitutive relation for surface viscosity $\gamma_s(\tilde{\Gamma}) \equiv \mu_s(\tilde{\Gamma}) + \mu_d(\tilde{\Gamma})$ or equivalently the Boussinesq-Scriven number $B_u \equiv \gamma_s/\mu h_c$ [recall Eq. (21)] is necessary in numerical simulations, the analytical formulas presented in this paper that account for the presence of surface viscous effects, and provide the necessary modifications to the results by Thete *et al.* [40] and Vaynblat *et al.* [38] for clean interfaces, can yet be generalized further without relying on any specific constitutive relation. Therefore, rather than assuming the linear relation that $B_u = B_r\Gamma/\Gamma_r = B_0\Gamma$, one can take $B_u = B_r f(\Gamma)$ where the function f is such that it equals unity at the reference surfactant concentration, viz. $f(\Gamma_r) = 1$, and vanishes when surfactant concentration equals zero, viz. $f(0) = 0$. A Taylor series expansion of $f(\Gamma)$ about $\Gamma = 0$ then reveals that

$$f(\Gamma) = f(0) + \left.\frac{df}{d\Gamma}\right|_{\Gamma=0} \Gamma + O(\Gamma^2) = f'(0)\Gamma + \ldots \tag{72}$$

Thus, $B_u = B_r f'(0)\Gamma$ as $\Gamma \to 0$ in the rupture zone. Hence, the generalization of the results given earlier but now without any dependence whatsoever on a particular constitutive relation can be obtained by replacing B_0 by $B_r f'(0)$ in χ.

VIII. CONCLUSIONS

In this paper, the thinning and rupture of thin liquid sheets of incompressible Newtonian fluids whose two free surfaces are covered with a monolayer of insoluble surfactant have been analyzed when surfactant convection is dominant over surfactant diffusion, viz. the Peclet number Pe $\gg 1$, and surface rheological effects are important. The dynamics close to the space-time rupture singularity has been analyzed both theoretically and by simulation when Pe = ∞. The dynamics in the vicinity of singularity has also been analyzed by simulation when Pe $\gg 1$ and the local dynamics

has been shown to be the same as when $\mathrm{Pe} = \infty$. Thus, in the remainder of this section, discussion of our new findings pertain to situations in which $\mathrm{Pe} = \infty$. In carrying out both the theoretical analysis and the simulations, advantage has been taken of the film's slenderness—the initial film half-thickness $\tilde{h}_i$ is much smaller than the wavelength of the perturbation causing instability of the sheet—and solving a long-wavelength model composed of a system of one-dimensional evolution partial differential equations for the film half-thickness $\tilde{h}(\tilde{z}, \tilde{t})$, lateral velocity $\tilde{v}(\tilde{z}, \tilde{t})$ and surfactant concentration $\tilde{\Gamma}(\tilde{z}, \tilde{t})$ where $\tilde{z}$ is the lateral coordinate and $\tilde{t}$ is time. As the dynamics near the space-time singularity where the film ruptures is asymptotically self-similar when surfactants are convected away from the rupture point, the partial differential evolution equations are also reduced to a set of ordinary differential equations in similarity space. Specifically, the dynamics has been analyzed in two distinct situations: one when inertia is negligible so that the sheet is undergoing Stokes flow and another when inertia cannot be neglected (inertial-viscous flow).

In both situations, it has been shown that the dominant balance of forces involves van der Waals, (bulk) viscous and surface viscous forces—inertia also enters the dominant balance when the sheet is undergoing inertial-viscous flow—while capillary (surface tension) and Marangoni forces are negligible as the sheet thins and tends toward rupture. For both sheets undergoing Stokes and inertial-viscous flow, similarity solutions have been obtained for the problem variables that have power-law dependencies on time remaining until rupture $\tilde{\tau}$ and are of the form given by the product of a scaling function multiplied by $\tilde{\tau}$ raised to some power (scaling exponent). In Stokes flow, the dynamics is shown to exhibit self-similarity of the second kind [39] and the power-law dependencies are given by

$$\tilde{h} \sim \tilde{\tau}^{1/3}, \quad \tilde{\Gamma} \sim \tilde{\tau}^{1/3}, \quad \tilde{z} \sim \tilde{\tau}^{0.249}, \quad \tilde{v} \sim \tilde{\tau}^{-0.751}, \tag{73}$$

and in inertial-viscous flow, the dynamics entails self-similarity of the first kind [39] and the power-law dependencies are given by

$$\tilde{h} \sim \tilde{\tau}^{1/3}, \quad \tilde{\Gamma} \sim \tilde{\tau}^{1/3}, \quad \tilde{z} \sim \tilde{\tau}^{1/2}, \quad \tilde{v} \sim \tilde{\tau}^{-1/2}. \tag{74}$$

In both situations, expressions have also been derived from theory for the minimum sheet half-thickness $\tilde{h}_{\min}$, results that are likely to be of great value to experimentalists who would be interested in measuring the temporal evolution of $\tilde{h}_{\min}$ and/or the sheet's thinning rate, i.e., the time derivative of $\tilde{h}_{\min}$. In Stokes flow, the sheet half-thickness has been shown to be given by [cf. Eq. (53)]

$$\frac{\tilde{h}_{\min}}{\tilde{h}_i} = \left(\frac{9}{4(6\alpha_z + 1)\chi}\right)^{1/3} \tau^{1/3} = 0.966\chi^{-1/3}\left(\frac{\tilde{\tau}}{t_{\mathrm{vis}}}\right)^{1/3}, \tag{75}$$

where $\alpha_z = 0.249$, and in inertial-viscous flow, the sheet half-thickness has been shown to be given by [cf. Eq. (76)]

$$\frac{\tilde{h}_{\min}}{\tilde{h}_i} = \frac{0.7401}{\mathrm{Oh}^{1/3}\chi^{1/3}}\left(\frac{\tilde{\tau}}{t_{\mathrm{cap}}}\right)^{1/3}, \tag{76}$$

where $\mathrm{Oh} = \mu/\sqrt{\rho\tilde{h}_i\sigma_p}$ is the Ohnesorge number. In both expressions, $\chi \equiv 1 + B_0 c_0/4$ where $B_0 \equiv B_r/\Gamma_0$, with $B_r \equiv \gamma_{sr}/\mu\tilde{h}_i$ standing for the reference Boussinesq-Scriven number, B_0 standing for the normalized reference Boussinesq-Scriven number, γ_{sr} denoting the reference value of the surface viscosity evaluated at $\Gamma = \Gamma_0$, and $c_0 \equiv \Gamma_0/h_0$ (h_0: initial minimum value of the film half-thickness upon the imposition of a sinusoidal perturbation of the sheet's surface at $t = 0$ which corresponds to the location where the film will rupture). In the expression for χ, $B_0 c_0/4$ represents the relative importance of surface viscous force to its bulk counterpart to leading order near the space-time singularity. The latter makes plain that surface rheological effects indeed compete with their bulk counterparts as $\tilde{\tau} \to 0$. A similar outcome has already been observed in pinch-off of surfactant-covered Newtonian jets/threads of highly viscous fluids undergoing Stokes flow (limit of zero density or negligible inertia) [47] and moderately viscous fluids undergoing inertial-viscous flow (situations in which inertia is nonnegligible) [48].

Given the aforementioned findings, it is appropriate to compare the results obtained in this paper with those reported in Refs. [41] and [42] in which the authors also considered the role of surface rheology in sheet rupture. As has already been explained in previous sections, the primary difference between the three works stems from the constitutive relation used to relate surface viscosity and surfactant concentration. In this paper, we, as in several recent papers on the subject [47–49,60], have adopted the physically-based ansatz that surface viscosity varies linearly with surfactant concentration. Moreover, it has been shown in Sec. VII that because surfactant evacuates the location where sheet thickness is a minimum, surface viscosity γ_s varies linearly with surfactant concentration $\tilde{\Gamma}$ as the sheet approaches rupture regardless of the constitutive equation used to relate γ_s and $\tilde{\Gamma}$. Therefore, the Boussinesq-Scriven number that measures the relative importance of surface viscous and viscous forces is given by $B_u = B_0\Gamma$. By contrast, Matar [41] took surface viscosity to be a constant regardless of surfactant concentration. However, Choudhury *et al.* [42] adopted a functional form for surface viscosity such that $B_u = B_0[1 + \beta(\Gamma - 1)]$ where $0 \leqslant \beta \leqslant 1$. When $\beta = 1$, their expressions for surface viscosity and hence Boussinesq-Scriven number become identical to ours. The limit of $\beta = 0$ reduces to the case analyzed by Matar [41]. Thus, the expressions for the surface viscosity adopted by Matar [41] ($\beta = 0$) and by Choudhury *et al.* [42] when $\beta \neq 1$ are physically unrealistic because they predict that γ_s is nonzero even at locations on the interface where surfactant concentration is identically zero. Moreover, Matar [41] and Choudhury *et al.* [42] did not address sheet rupture in the Stokes limit. Furthermore, regardless of whether sheet rupture takes place when inertia is negligible or important, the present paper is the only one to date that has provided an analytical expression for $h_{\min}$ as a function of τ or the sheet's thinning rate. Additionally, when $\beta = 1$, an incorrect conclusion was reached in Ref. [42] regarding the asymptotic balance of forces that exists as the sheet tends toward rupture. A succinct summary of all of these findings is presented in Fig. 8.

The dynamics of thinning and rupture of liquid sheets with clean interfaces as well as ones with surfactant-covered interfaces in the presence of surface viscous effects can be conveniently displayed in a single phase diagram as shown in Fig. 9. Based on experience with other interfacial flows with pinch-off singularities such as jet/drop breakup [66], it turns out to be convenient here to construct such a diagram in the $(B_{\rm loc}, \mathrm{Re})$ phase space. Here, Re is the Reynolds number, which is the reciprocal of the Ohnesorge number Oh, and $B_{\rm loc}$ is the local Boussinesq-Scriven number given by $B_{\rm loc} = B_u/h$. It should be noted that the Reynolds number is either $\mathrm{Re} = 0$ or $\mathrm{Re} \sim 1$ or $\mathrm{Re} = \infty$. The local Boussinesq-Scriven number is the instantaneous value of the ratio of the surface viscous to bulk viscous stress in the rupture zone. In this work, $B_{\rm loc} = B_0\Gamma/h$. Since both Γ and h scale as $\tau^{1/3}$, $B_{\rm loc} \sim 1$ throughout the time that the sheet is thinning and tending toward rupture, viz. surface and bulk viscous forces remain in balance as the sheet tends toward breakup. In Refs. [41,42], $B_{\rm loc} = B_0[1 + \beta(\Gamma - 1)]/h$. Since $\beta = 0$ in Ref. [41] and when $\beta \neq 1$ in Ref. [42], $B_{\rm loc} \to \infty$ as the sheet tends toward rupture or as $h \to 0$. Although mathematically correct, this portion of the phase space is unlikely to be attained in practice because surface viscosity cannot be constant or be nonzero where surfactant concentration vanishes. For sheets with clean as well as surfactant-covered interfaces, transitions are possible from initial regimes that are either bulk-viscous force or inertia dominated to ones where bulk-viscous and inertial forces are equally important, as discussed earlier and shown in Fig. 9.

In this paper, sheet thinning and rupture have been considered for two-dimensional perturbations as opposed to axisymmetric ones which lead to the film rupturing at a point. In the literature on the thinning and rupture of free and supported films of Newtonian fluids, researchers have studied both types of rupture. Vaynblat *et al.* [38] state that sheet rupture is unstable to perturbations in the transverse direction, as capillary force would be too weak to stabilize the film against them. We shall report in a future publication results on the analogous problem of axisymmetric or point rupture of surfactant-covered liquid sheets.

In the presence of surfactants, surface tension has a value that is lower than that when the interface is devoid of surfactant and is reduced by an amount that depends on the local concentration of surfactant. As summarized in a countless number of review articles and monographs

Publication	Key results/ conclusions	Stokes flow	Inertial-viscous flow
Matar $(\beta \equiv 0)$	Power-law dependencies Dominant balance of forces Analytical formula for the thinning rate with prefactor	No	$h \sim \tau^{1/2}$, $\Gamma \sim \tau^{1/2}$, $z \sim \tau^{1/4}$, $v \sim \tau^{-3/4}$ vdW ~ I ~ SV No
Choudhoury et al. $(0 \leq \beta < 1)$		No	$h \sim \tau^{1/2}$, $\Gamma \sim \tau^{1/2}$, $z \sim \tau^{1/4}$, $v \sim \tau^{-3/4}$ vdW ~ I ~ SV No
Choudhoury et al. $(\beta = 1)$		No	$h \sim \tau^{1/3}$, $\Gamma \sim \tau^{1/3}$, $z \sim \tau^{1/2}$, $v \sim \tau^{-1/2}$ vdW ~ I ~ SV No
This work		$h \sim \tau^{1/3}$, $\Gamma \sim \tau^{1/3}$, $z \sim \tau^{0.249}$, $v \sim \tau^{-0.751}$ vdW ~ V ~ SV $h_{min} = \left(\frac{9}{4\,(6\alpha_z + 1)\,\chi}\right)^{1/3} \tau^{1/3}$	$h \sim \tau^{1/3}$, $\Gamma \sim \tau^{1/3}$, $z \sim \tau^{1/2}$, $v \sim \tau^{-1/2}$ vdW ~ V ~ I ~ SV $h_{min} = \frac{0.7401}{(\chi \mathrm{Oh})^{1/3}} \tau^{1/3}$

FIG. 8. Publications in which the thinning and rupture of free films of Newtonian fluids have been analyzed in situations in which the sheets' two free surfaces are covered with insoluble surfactant and surface rheological effects are important when Pe $\gg 1$ (surfactant convection is dominant over surfactant diffusion). In this figure, Matar and Choudhoury *et al*. denote Refs. [41] and [42]. Listed here are three key results and/or conclusions that have been obtained in these papers: (i) the power-law dependencies of key variables (in black font), i.e., the variation with time remaining to rupture τ of the sheet half-thickness h, surfactant concentration Γ, lateral length z, and lateral velocity v, (ii) the dominant balance of forces (in red font), and (iii) the theoretically predicted thinning rate which is given by the time derivative of h_{min} (in blue font). In this and the next figure, vdW, I, V, SV, and ST denote van der Waals, inertial, (bulk) viscous, surface viscous, and surface tension (capillary) forces. The Stokes limit has not been considered in Refs. [41] and [42]. Furthermore, theoretical expressions for the sheet's thinning rate are not reported in Refs. [41] and [42] when the sheet is undergoing inertial-viscous flow.

[19,29,67–69], there now exist dozens of methods for accurately measuring the surface tension of clean as well as surfactant-covered interfaces. In the presence of surface rheological effects, the standard approach, which has also been adopted in this manuscript, has consisted of describing the interface as a compressible two-dimensional Newtonian fluid with surface shear and dilatational viscosities obeying the Boussinesq-Scriven equations [58]. However, in contrast to measuring the value of surface tension, measurement of material properties of interfaces has proven challenging and elusive [70]. For example, Stevenson [71] has articulated in a review article that researchers have reported measured values of surface shear viscosity that differ by orders of magnitude. One possible culprit for the discrepancies in measurements may be that many experimental methods generate a mixed interfacial flow, with both shear and dilatational components, and the surface shear and dilatational viscosities cannot be uniquely determined from measurements of a single mixed-type flow [28]. Another culprit may be that the flows induced in different experiments often give rise to gradients in surface tension which then makes it virtually impossible to separate the contributions of the resulting Marangoni stresses from those due to surface viscosities. Given the fact that Marangoni stresses become negligible compared to surface viscous stresses in sheet rupture, thinning liquid sheets can provide a convenient experimental platform for inferring surface viscosities by using Eq. (75) or Eq. (76) (also, see below).

While many of the key results in this theoretical and computational study have been presented in terms of dimensionless variables, it is of interest to briefly address what might be observed in laboratory experiments where it would be necessary to consider the actual values of physical

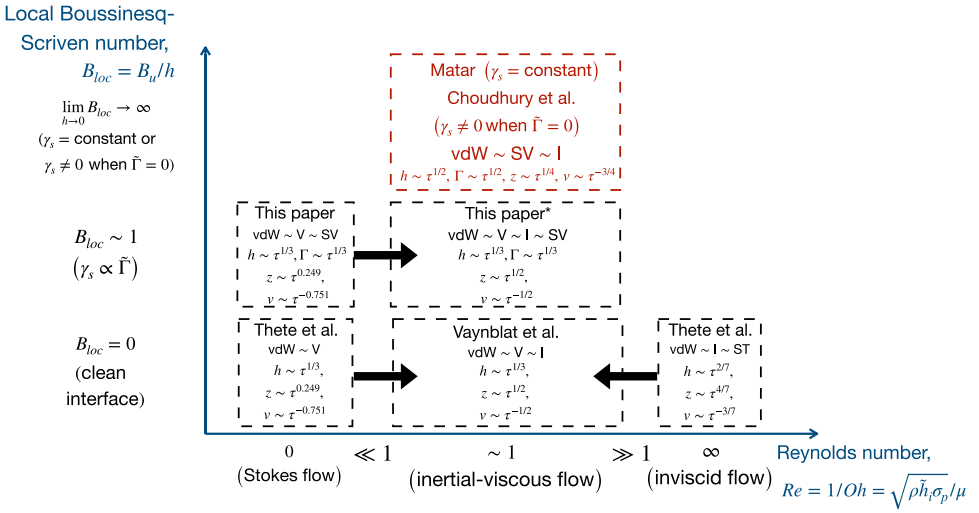

FIG. 9. Summary of the dynamical responses of liquid sheets undergoing van der Waals driven thinning and rupture: phase diagram in ($B_{\rm loc}$, Re) space. In this figure, Matar, Choudhoury *et al.*, Vaynblat *et al.*, and Thete *et al.* denote Refs. [41], [42], [38], and [40]. Theoretical scaling laws exist when $\mathrm{Re} = 0$ ($\mathrm{Oh} = \infty$), $\mathrm{Re} \sim 1$ ($\mathrm{Oh} \sim 1$), and $\mathrm{Re} = \infty$ ($\mathrm{Oh} = 0$), and are now known in these limits for sheets with both clean interfaces ($B_{\rm loc} = 0$) and ones that are covered with a monolayer of insoluble surfactant in the presence of surface viscous effects. The inertial-viscous scaling regime in the limit of $B_{\rm loc} \to \infty$, highlighted in red, constitutes a mathematically correct solution of the governing equations but may be unattainable in practice because of the aphysical nature of the relationship between surface viscosity and surfactant concentration that was assumed in those papers, i.e., $\gamma_s =$ constant or $\gamma_s \neq 0$ when $\tilde{\Gamma} = 0$. The star in the box in the middle of the diagram ("This paper*") indicates that the power-law dependencies for the regime where ($B_{\rm loc} \sim 1$, $\mathrm{Re} \sim 1$) for which $\gamma_s \propto \tilde{\Gamma}$ have also been obtained in Ref. [42] but the authors of that paper have incorrectly concluded that surface viscous force is negligible at the incipience of sheet rupture and have not reported an exact analytical expression for the sheet's thinning rate as has been done in this paper. Reynolds (Ohnesorge) number cannot equal zero or infinity in real systems. Thus, for systems for which $\mathrm{Re} \ll 1$ ($\mathrm{Oh} \gg 1$) or $\mathrm{Re} \gg 1$ ($\mathrm{Oh} \ll 1$), the dynamics would transition from an initial Stokes or inviscid scaling regime to a final inertial-viscous scaling regime as indicated by the arrows in the figure.

properties and film thickness. Since glycerol-water solutions are some of the most commonly used fluids in studies of pinch-off singularities [24,50,72], we use such mixtures in the numerical example that will be provided. Hence, we consider two liquid sheets of identical initial film half-thickness of $\tilde{h}_i = 1$ μm where the solvent in one case is water and the other a glycerol-water solution of viscosity fifty times that of water [50]. For the sheet for which the solvent is water, $\mathrm{Oh} = 0.12$. As shown in this paper, as rupture nears, such a liquid sheet would thin and break up in the inertial-viscous regime, as summarized in Figs. 8 and 9. If, however, the solvent is the glycerol-water solution that is 50 times more viscous than water, then $\mathrm{Oh} = 6$. After the decay of initial transients, such a liquid sheet would initially thin in the viscous or Stokes regime. As per the results presented in Sec. III E and Eq. (56), the dynamics would then transition to the inertial-viscous regime when the minimum value of the sheet's half-thickness falls below about 93 nm. The measured rates of thinning in both regimes can then be used to determine the surface viscosities of the surfactant-covered sheets of water and the glycerol-water solution that is fifty times more viscous than water.

Despite the aforementioned challenges in accurately measuring surface viscosity, it would also be valuable to experimentalists as well as practitioners to include here a discussion of the order of magnitude of the Boussinesq-Scriven number B_u based on realistic values of physical properties. Typical values of the surface viscosity lie in the range 10^{-8}–10^{-6} Pa m s [71,73,74] and those of

the viscosity of glycerol-water solutions are in the range of 10^{-3}–10^{-1} Pa s. If the liquid sheet's initial film half-thickness is 1 μm, then the order of magnitude of the Boussinesq-Scriven number for such systems would be in the range of 10^{-1}–10^{3}. Therefore, in all simulation results reported in the present study, the value of B_u at the initial surfactant coverage was chosen to lie roughly in the middle of this range, i.e., between 1 and 10.

ACKNOWLEDGMENTS

The authors thank the Purdue Process Safety and Assurance Center (P2SAC), the Bilsland Dissertation Fellowship to B.W.W., and the Gedge Professorship to O.A.B. for financial support. The authors report no conflict of interest.

[1] A. Oron, S. H. Davis, and S. G. Bankoff, Long-scale evolution of thin liquid films, Rev. Mod. Phys. **69**, 931 (1997).
[2] G. F. Teletzke, H. T. Davis, and L. E. Scriven, How liquids spread on solids, Chem. Eng. Commun. **55**, 41 (1987).
[3] D. Lohse and E. Villermaux, Double threshold behavior for breakup of liquid sheets, Proc. Natl. Acad. Sci. USA **117**, 18912 (2020).
[4] P.-G. de Gennes, Wetting: Statics and dynamics, Rev. Mod. Phys. **57**, 827 (1985).
[5] H. S. Kheshgi and L. E. Scriven, Dewetting: Nucleation and growth of dry regions, Chem. Eng. Sci. **46**, 519 (1991).
[6] B. Néel and E. Villermaux, The spontaneous puncture of thick liquid films, J. Fluid Mech. **838**, 192 (2018).
[7] G. Debrégeas, P.-G. De Gennes, and F. Brochard-Wyart, The life and death of "bare" viscous bubbles, Science **279**, 1704 (1998).
[8] S. Cohen-Addad, R. Höhler, and O. Pitois, Flow in foams and flowing foams, Annu. Rev. Fluid Mech. **45**, 241 (2013).
[9] Y. Yoon, F. Baldessari, H. D. Ceniceros, and L. G. Leal, Coalescence of two equal-sized deformable drops in an axisymmetric flow, Phys. Fluids **19**, 102102 (2007).
[10] K. Sambath, V. Garg, S. S. Thete, H. J. Subramani, and O. A. Basaran, Inertial impedance of coalescence during collision of liquid drops, J. Fluid Mech. **876**, 449 (2019).
[11] D. Langevin, Bubble coalescence in pure liquids and in surfactant solutions, Curr. Opin. Colloid Interface Sci. **20**, 92 (2015).
[12] Z. Tadmor and C. G. Gogos, *Principles of Polymer Processing* (John Wiley & Sons, New York, NY, 2013)
[13] M. S. Bazzi and M. S. Carvalho, Effect of viscoelasticity on liquid sheet rupture, J. Non-Newtonian Fluid Mech. **264**, 107 (2019).
[14] S. F. Kistler and L. E. Scriven, Coating flows, in *Computational Analysis of Polymer Processing* (Springer, Berlin, 1983), pp. 243–299.
[15] S. J. Weinstein and K. J. Ruschak, Coating flows, Annu. Rev. Fluid Mech. **36**, 29 (2004).
[16] R. J. Braun, Dynamics of the tear film, Annu. Rev. Fluid Mech. **44**, 267 (2012).
[17] R. Sijs, S. Kooij, and D. Bonn, How surfactants influence the drop size in sprays from flat fan and hollow cone nozzles, Phys. Fluids **33**, 113608 (2021).
[18] P. R. Schunk and L. E. Scriven, Surfactant effects in coating processes, in *Liquid Film Coating* (Springer, Berlin, 1997), pp. 495–536.
[19] J. C. Berg, *An Introduction to Interfaces & Colloids: The Bridge to Nanoscience* (World Scientific, Singapore, 2010).
[20] C. V. Sternling and L. E. Scriven, Interfacial turbulence: Hydrodynamic instability and the Marangoni effect, AIChE J. **5**, 514 (1959).
[21] L. E. Scriven and C. V. Sternling, The Marangoni effects, Nature (London) **187**, 186 (1960).

[22] D. Lohse and X. Zhang, Physicochemical hydrodynamics of droplets out of equilibrium, Nat. Rev. Phys. **2**, 426 (2020).
[23] P. T. McGough and O. A. Basaran, Repeated Formation of Fluid Threads in Breakup of a Surfactant-Covered Jet, Phys. Rev. Lett. **96**, 054502 (2006).
[24] P. M. Kamat, B. W. Wagoner, S. S. Thete, and O. A. Basaran, Role of Marangoni stress during breakup of surfactant-covered liquid threads: Reduced rates of thinning and microthread cascades, Phys. Rev. Fluids **3**, 043602 (2018).
[25] Y. Li, C. Diddens, A. Prosperetti, K. L. Chong, X. Zhang, and D. Lohse, Bouncing Oil Droplet in a Stratified Liquid and its Sudden Death, Phys. Rev. Lett. **122**, 154502 (2019).
[26] A. Marin, S. Karpitschka, D. Noguera-Marín, M. A. Cabrerizo-Vílchez, M. Rossi, C. J. Kähler, and M. A. Rodriguez Valverde, Solutal Marangoni flow as the cause of ring stains from drying salty colloidal drops, Phys. Rev. Fluids **4**, 041601(R) (2019).
[27] D. Lohse, Fundamental fluid dynamics challenges in inkjet printing, Annu. Rev. Fluid Mech. **54**, 349 (2022).
[28] G. J. Elfring, L. G. Leal, and T. M. Squires, Surface viscosity and Marangoni stresses at surfactant laden interfaces, J. Fluid Mech. **792**, 712 (2016).
[29] Y. M. Tricot, Surfactants: Static and dynamic surface tension, in *Liquid Film Coating: Scientific Principles and Their Technological Implications*, edited by S. F. Kistler and P. M. Schweizer (Springer, Netherlands, 1997), pp. 99–136.
[30] B. Scheid, J. Delacotte, B. Dollet, E. Rio, F. Restagno, E. A. Van Nierop, I. Cantat, D. Langevin, and H. A. Stone, The role of surface rheology in liquid film formation, Europhys. Lett. **90**, 24002 (2010).
[31] B. Scheid, S. Dorbolo, L. R. Arriaga, and E. Rio, Antibubble Dynamics: The Drainage of an Air Film with Viscous Interfaces, Phys. Rev. Lett. **109**, 264502 (2012).
[32] A. Sheludko, Certain peculiarities of foam lamellas, Parts I–III, in *Proc. Koninkl. Ned. Akad. Wetenschap. B*, Vol. 65 (1962) pp. 76–108.
[33] A. Vrij, Possible mechanism for the spontaneous rupture of thin, free liquid films, Discuss. Faraday Soc. **42**, 23 (1966).
[34] A. Sheludko, Thin liquid films, Adv. Colloid Interface Sci. **1**, 391 (1967).
[35] E. Ruckenstein and R. K. Jain, Spontaneous rupture of thin liquid films, J. Chem. Soc., Faraday Trans. 2 **70**, 132 (1974).
[36] T. Erneux and S. H. Davis, Nonlinear rupture of free films, Phys. Fluids A **5**, 1117 (1993).
[37] M. P. Ida and M. J. Miksis, Thin film rupture, Appl. Math. Lett. **9**, 35 (1996).
[38] D. Vaynblat, J. R. Lister, and T. P. Witelski, Rupture of thin viscous films by van der Waals forces: Evolution and self-similarity, Phys. Fluids **13**, 1130 (2001).
[39] G. I. Barenblatt, *Scaling, Self-similarity, and Intermediate Asymptotics: Dimensional Analysis and Intermediate Asymptotics*, Cambridge Texts in Applied Mathematics (Cambridge University Press, Cambridge, UK, 1996).
[40] S. S. Thete, C. Anthony, P. Doshi, M. T. Harris, and O. A. Basaran, Self-similarity and scaling transitions during rupture of thin free films of newtonian fluids, Phys. Fluids **28**, 092101 (2016).
[41] O. K. Matar, Nonlinear evolution of thin free viscous films in the presence of soluble surfactant, Phys. Fluids **14**, 4216 (2002).
[42] A. Choudhury, V. K. Paidi, S. K. Kalpathy, and H. N. Dixit, Enhanced stability of free viscous films due to surface viscosity, Phys. Fluids **32**, 082108 (2020).
[43] J. C. Burton and P. Taborek, Two-dimensional inviscid pinch-off: An example of self-similarity of the second kind, Phys. Fluids **19**, 102109 (2007).
[44] J. Eggers and M. A. Fontelos, *Singularities: Formation, Structure, and Propagation* (Cambridge University Press, Cambridge, UK, 2015).
[45] M. Bowen and B. S. Tilley, On self-similar thermal rupture of thin liquid sheets, Phys. Fluids **25**, 102105 (2013).
[46] G. Kitavtsev, M. A. Fontelos, and J. Eggers, Thermal rupture of a free liquid sheet, J. Fluid Mech. **840**, 555 (2018).

[47] H. Wee, B. W. Wagoner, P. M. Kamat, and O. A. Basaran, Effects of Surface Viscosity on Breakup of Viscous Threads, Phys. Rev. Lett. **124**, 204501 (2020).
[48] H. Wee, B. W. Wagoner, V. Garg, P. M. Kamat, and O. A. Basaran, Pinch-off of a surfactant-covered jet, J. Fluid Mech. **908**, A38 (2021).
[49] H. Wee, B. W. Wagoner, and O. A. Basaran, Absence of scaling transitions in breakup of liquid jets caused by surface viscosity, Phys. Rev. Fluids **7**, 074001 (2022).
[50] Y. C. Liao, E. I. Franses, and O. A. Basaran, Deformation and breakup of a stretching liquid bridge covered with an insoluble surfactant monolayer, Phys. Fluids **18**, 022101 (2006).
[51] F. Brochard-Wyart, J.-M. di Meglio, D. Quére, and P.-G. de Gennes, Spreading of nonvolatile liquids in a continuum picture, Langmuir **7**, 335 (1991).
[52] V. Bergeron, Disjoining pressures and film stability of alkyltrimethylammonium bromide foam films, Langmuir **13**, 3474 (1997).
[53] B. Dai and L. G. Leal, The mechanism of surfactant effects on drop coalescence, Phys. Fluids **20**, 040802 (2008).
[54] C. Vannozzi, Coalescence of surfactant-covered drops in extensional flows: Effects of the interfacial diffusivity, Phys. Fluids **24**, 082101 (2012).
[55] D. T. Papageorgiou, On the breakup of viscous liquid threads, Phys. Fluids **7**, 1529 (1995).
[56] H. A. Stone, A simple derivation of the time-dependent convective-diffusion equation for surfactant transport along a deforming interface, Phys. Fluids **2**, 111 (1990).
[57] R. Aris, *Vectors, Tensors, and the Basic Equations of Fluid Mechanics* (Courier Corporation, North Chelmsford, MA, 2012).
[58] L. E. Scriven, Dynamics of a fluid interface equation of motion for Newtonian surface fluids, Chem. Eng. Sci. **12**, 98 (1960).
[59] B. Ambravaneswaran and O. A. Basaran, Effects of insoluble surfactants on the nonlinear deformation and breakup of stretching liquid bridges, Phys. Fluids **11**, 997 (1999).
[60] A. Ponce-Torres, J. M. Montanero, M. A. Herrada, E. J. Vega, and J. M. Vega, Influence of the Surface Viscosity on the Breakup of a Surfactant-Laden Drop, Phys. Rev. Lett. **118**, 024501 (2017).
[61] M. Bowen and B. S. Tilley, Thermally induced van der Waals rupture of thin viscous fluid sheets, Phys. Fluids **24**, 032106 (2012).
[62] J. Eggers, Universal Pinching of 3D Axisymmetric Free-Surface Flow, Phys. Rev. Lett. **71**, 3458 (1993).
[63] J. Eggers, Drop formation–an overview, ZAMM-J. App. Math. Mech. **85**, 400 (2005).
[64] S. S. Thete (private communication).
[65] B. W. Wagoner, S. S. Thete, and O. A. Basaran, A new experimental method based on volume measurement for determining axial scaling during breakup of drops and liquid threads, Phys. Fluids **30**, 082102 (2018).
[66] J. R. Castrejón-Pita, A. A. Castrejón-Pita, S. S. Thete, K. Sambath, I. M. Hutchings, J. Hinch, J. R. Lister, and O. A. Basaran, Plethora of transitions during breakup of liquid filaments, Proc. Natl. Acad. Sci. USA **112**, 4582 (2015).
[67] X. Zhang, M. T. Harris, and O. A. Basaran, Measurement of dynamic surface tension by a growing drop technique, J. Colloid Interface Sci. **168**, 47 (1994).
[68] E. I. Franses, O. A. Basaran, and C. H. Chang, Techniques to measure dynamic surface tension, Curr. Opin. Colloid Interface Sci. **1**, 296 (1996).
[69] M. Hoorfar and A. W. Neumann, Recent progress in axisymmetric drop shape analysis (ADSA), Adv. Colloid Interface Sci. **121**, 25 (2006).
[70] J. M. Lopez and A. Hirsa, Direct determination of the dependence of the surface shear and dilatational viscosities on the thermodynamic state of the interface: Theoretical foundations, J. Colloid Interface Sci. **206**, 231 (1998).
[71] P. Stevenson, Remarks on the shear viscosity of surfaces stabilised with soluble surfactants, J. Colloid Interface Sci. **290**, 603 (2005).
[72] P. M. Kamat, B. W. Wagoner, A. A. Castrejón-Pita, J. R. Castrejón-Pita, C. R. Anthony, and O. A. Basaran, Surfactant-driven escape from endpinching during contraction of nearly inviscid filaments, J. Fluid Mech. **899**, A28 (2020).

[73] O. Pitois, C. Fritz, and M. Vignes-Adler, Liquid drainage through aqueous foam: Study of the flow on the bubble scale, J. Colloid Interface Sci. **282**, 458 (2005).

[74] Z. A. Zell, A. Nowbahar, V. Mansard, L. G. Leal, S. S. Deshmukh, J. M. Mecca, C. J. Tucker, and T. M. Squires, Surface shear inviscidity of soluble surfactants, Proc. Natl. Acad. Sci. USA **111**, 3677 (2014).